DESY PRC 01-01
HERMES 01-017
April 2001

A Large Acceptance Recoil Detector for HERMES

Addendum to the Proposal DESY PRC 97-07, HERMES 97-032

The HERMES Collaboration *

* Contact Person: R. Kaiser, University of Glasgow,
email: r.kaiser@physics.gla.ac.uk, phone: ++44-141-330 5287

Abstract

In 1997 the HERMES collaboration proposed to build a silicon-detector system for the HERMES front region in the vicinity of the internal storage cell target, consisting of the so-called 'Λ-wheels' and a Recoil Detector. The Λ-wheels have been installed and will be commissioned this fall. For the Recoil Detector the focus of the physics case has been shifted from tagged structure functions and J/ψ production to Skewed Parton Distributions (SPDs) and hard exclusive reactions, e.g. Deeply Virtual Compton scattering (DVCS). This calls for a Recoil Detector with a much larger acceptance in both polar and azimuthal angle as well as momentum. This paper outlines the physics prospects of HERMES with the new large acceptance Recoil Detector as well as its conceptual design. The Recoil Detector will include a silicon tracker inside the beam vacuum for the detection of the lower momentum recoil protons, similar to the Recoil Detector of the 1997 proposal but with an increased acceptance. In addition there will be a scintillating fibre tracker in a longitudinal magnetic field for the detection of the higher momentum recoil protons. The Recoil Detector will be completed by a γ-detector that uses the return yoke of the magnet as preshower material. This γ-detector will help to further reduce the background by detecting π^0 mesons from the decay of Δ resonances.

Contents

1 Introduction

In 1997 the HERMES collaboration proposed to build a silicon-detector system for the HERMES front region in the vicinity of the internal storage cell target [1]. This detector should consist of two components:

(1) Two wheel-shaped arrays of double-sided silicon counters, the so-called 'Λ-wheels', placed within the pumping cross of the target chamber. They should mainly serve to increase the acceptance for Λ-particles and to decrease the false asymmetry in the determination of the Λ-polarisation. In this way they greatly increase the prospects for Λ-physics. In the meantime this detector has been installed and will be commissioned after the long HERA shutdown 2000/01.

(2) A set of silicon-strip detectors, the so-called 'Recoil Detector', positioned within the target chamber parallel above (and below) the storage cell such that they cover part of the backward hemisphere. Since the gas target is very dilute and the walls of the storage cell are very thin (50-75μm) they should allow to detect very low momentum recoil products. This includes recoil protons in exclusive diffractive reactions or spectator protons in deep-inelastic scattering processes from neutrons in a deuteron target.

A silicon test counter [2,3], a telescope consisting of two double-sided silicon counters with a thickness of 135 μm (300 μm) positioned 60 mm (75 mm) underneath the storage cell was installed in the HERMES target chamber in May 1998. It has been operated successfully for several months, demonstrating the technical feasibility of operating such a device under these particular conditions (ultra-high vacuum, severe radio-frequency and radiation background). The measurements with this test detector also demonstrated the capability of such a detector system to detect and identify very low momentum protons down to momenta of about 100 MeV/c and to measure their energy via the energy deposited in the two counters. As an example of the results the reconstructed momentum distribution of spectator protons originating from deep inelastic reactions on neutrons in a deuteron target is shown in figure 1. This is the first measurement of this distribution in deep-inelastic scattering and it agrees nicely with the parameterisation from low-energy experiments, represented by the solid line [4–6].

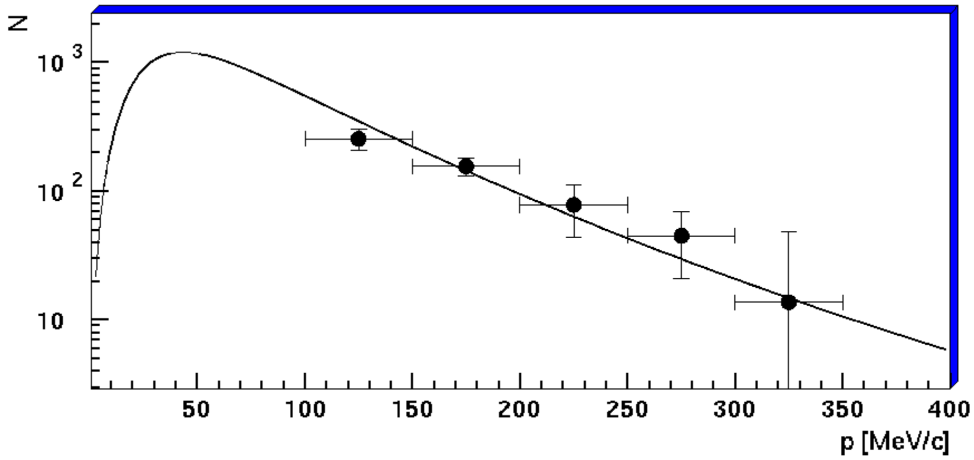

Fig. 1. Distribution of the reconstructed momentum of spectator protons from deep inelastic reactions on neutrons in a deuterium target.

At the time of the proposal of the original Recoil Detector, the main emphasis was on the identification of diffractive elastic J/ψ events and on the detection of spectator protons from a deuteron target. The first was meant to gain access to the polarised gluon distribution [7–9], while the detection of spectator protons would lead to an improved measurement of the neutron structure function $F_2^n(x)$ at large values of Bjorken-x [10,11]. It also would allow to study the origin of the EMC-effect [12].

In the meantime, however, it has become clear that there is an even more important physics case that requires the extension of the HERMES spectrometer by a Recoil Detector, namely the hard exclusive electroproduction of (pseudoscalar and vector) mesons and real photons (Deeply Virtual Compton Scattering - DVCS). The measurement of these hard exclusive reactions will give access to a new class of parton distributions, the so-called skewed parton distributions (SPD) (also referred to as off-forward or generalised parton distributions [13–16]). Among many different aspects these distributions open the possibility to access experimentally the total contribution J_q of quarks to the nucleon spin, including their orbital angular momenta [16].

HERMES already has observed and investigated the exclusive electroproduction of ρ-mesons [17,18], of charged and neutral pions [19] and the beam-spin azimuthal asymmetry associated with DVCS [20]. The missing mass resolution for such reactions is dominated by the momentum resolution of the forward spectrometer for charged tracks and the energy resolution of the lead-glass calorimeter for photons. This resolution is insufficient to unambiguously identify exclusive events with the target nucleon staying intact and to separate them from those where e.g. a Δ resonance is created. With the present spectrometer setup it is not possible to improve the momentum and energy resolution and thereby the separation of these channels. The identification of exclusive events can, however, be considerably improved by the here proposed Large Acceptance Recoil Detector. This can basically be done in two ways:

- Recoil proton detection.
  The recoil proton is identified and its momentum and angle is measured. This also requires the separation of recoil protons from background pions. Coplanarity cuts or an overall kinematic fit can then be used to select exclusive events.
- Hermeticity.
  Events with more than one particle in the c.m. backward hemisphere are excluded. This requires that the Recoil Detector should be as hermetic as possible, i.e. fully enclose the target cell, and its geometrical acceptance should connect to that of the Λ-wheels.

As will be shown in detail in section 3.1 the recoiling protons in the different aforementioned exclusive reactions cover a momentum range from about 100 MeV/c to beyond 1 GeV/c and a polar angular range up to about 1.35 rad. Compared to the original Recoil Detector design, this calls for a much larger acceptance in angle (polar and azimuthal) and momentum.

The following sections of this paper will first discuss the physics prospects in terms of the different processes that can be observed, the expected luminosity and competing experiments. This is followed by the conceptual design of the Large Acceptance Recoil Detector, consisting of a silicon tracker inside the beam vacuum, a scintillating fibre detector, a superconducting solenoidal magnet and a π^0-detector. The last sections are devoted to the planned background test experiment and an organisational overview of the project.

2 Physics Prospects

2.1 Skewed Parton Distributions

Traditionally, the investigation of the spin structure of the nucleon in electron scattering has been synonymous with inclusive measurements. In more recent times, semi-inclusive measurements have substantially extended the understanding of the nucleon spin. Now exclusive reactions are emerging as a possible way to complete the picture.

A unified theoretical description of inclusive and exclusive processes has been obtained through the formalism of generalised parton distributions, typically referred to as Skewed Parton Distributions (SPD) [13–16]. The usual parton distributions represent the probability to find a parton with specified longitudinal momentum fraction x in the fast moving hadron. SPDs, in contrast, represent the interference of different wave functions, one with a parton having momentum fraction $x+\xi$ and one with a parton having momentum fraction $x-\xi$. In addition, SPDs depend on a third variable besides the momentum fraction variables x and ξ, the momentum transfer $-t = \Delta^2 = (p-p')^2$ between two hadron states with momenta p and p', respectively.

There are four different types of quark SPDs that contribute to the simplest hard exclusive process - Deeply Virtual Compton Scattering (DVCS), $ep \longrightarrow ep\gamma$. The unpolarised distributions $H^q(x,\xi,\Delta^2)$ and $E^q(x,\xi,\Delta^2)$ and the polarised distributions $\widetilde{H}^q(x,\xi,\Delta^2)$ and $\widetilde{E}^q(x,\xi,\Delta^2)$. The skewed parton distributions offer a unified description of ordinary parton distributions and nucleon form factors. In the limit of $\Delta^2 \to 0$, $\xi \to 0$

$$H^q(x,0,0) = q(x), \quad \widetilde{H}^q(x,0,0) = \Delta q(x), \tag{1}$$

where $q(x)$ and $\Delta q(x)$ are the ordinary quark and quark helicity distributions. On the other hand, the first moments of the SPDs simplify to the flavour dependent form factors:

$$\begin{aligned}
\int_{-1}^{1} dx H^q(x,\xi,\Delta^2) &= F_1^q(\Delta^2) \\
\int_{-1}^{1} dx E^q(x,\xi,\Delta^2) &= F_2^q(\Delta^2) \\
\int_{-1}^{1} dx \widetilde{H}^q(x,\xi,\Delta^2) &= G_A^q(\Delta^2) \\
\int_{-1}^{1} dx \widetilde{E}^q(x,\xi,\Delta^2) &= G_P^q(\Delta^2)
\end{aligned} \tag{2}$$

where $F_1(\Delta^2)$ and $F_2(\Delta^2)$ are the Dirac and Pauli form factors and $G_A(\Delta^2)$ and $G_P(\Delta^2)$ are the axial-vector and pseudo-scalar form factors.

A strong motivation to study SPDs followed from the finding of Ji [16], who discovered that the second moment of the unpolarised SPDs H^q and E^q in the limit $\Delta^2 = 0$ is relevant to the spin structure of the nucleon and gives the gauge invariant total quark angular momentum:

$$J_q = \frac{1}{2}\int_{-1}^{+1} dx\, x \left[H^q(x,\xi,\Delta^2=0) + E^q(x,\xi,\Delta^2=0)\right] . \tag{3}$$

The quark angular momentum J_q decomposes as

$$J_q = \frac{1}{2}\Delta\Sigma + L_q \ , \tag{4}$$

where $\Delta\Sigma/2$ and L_q are the quark spin and the orbital angular momentum, respectively. As $\Delta\Sigma$ is measured through polarised DIS experiments, a measurement of the sum rule of equation (3) in terms of the SPDs provides a hitherto unique way to determine the quark orbital angular momentum contribution to the nucleon spin and thus, in principle, from

$$\frac{1}{2} = J_q + J_g \ , \tag{5}$$

the contribution of the total gluon angular momentum J_g. It should be noted that this requires access to both unpolarised SPDs, H^q and E^q, and that it is necessary to be able to extrapolate to $\Delta^2 = 0$. This stresses the importance of measurements at low values of $-t = \Delta^2$.

2.2 Deeply Virtual Compton Scattering

2.2.1 DVCS Basics

A particularly promising way of studying the nucleon structure is by means of deeply virtual Compton scattering (DVCS), where a virtual photon couples to the proton, and a real photon is emitted ($\gamma^* + p \to \gamma + p$). The proton is left intact. The DVCS process combines the advantages of deep inelastic scattering (DIS) and Compton scattering: The initial photon is off-shell, thus opening an additional dimensional parameter with respect to real Compton scattering. At the same time it is simpler than meson production in DIS because the composite meson in the final state is replaced by an elementary object, the photon, so that there is no meson wave function to be considered.

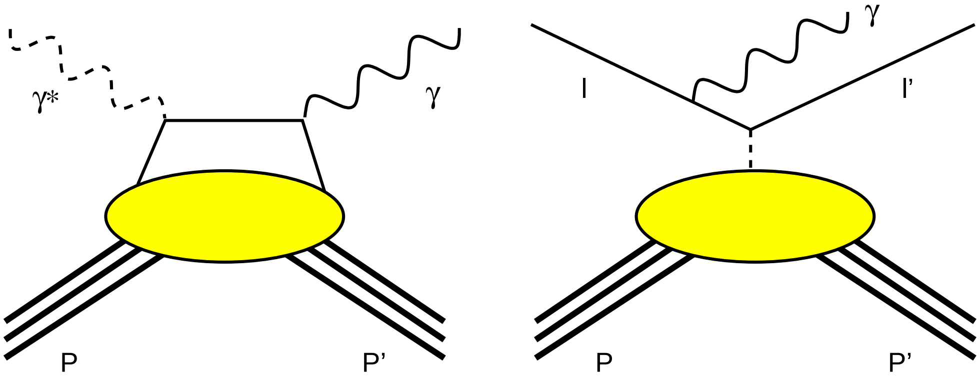

Fig. 2. Schematic DVCS handbag diagram (left) and one of the diagrams for the competing Bethe-Heitler process (right).

A general framework for exclusive processes at high values of Q^2 was first developed by Brodsky and Lepage [21], wherein the scattering process is separated into a hard part that describes the interaction of the virtual photon with a single quark and a soft part that contains the wave functions of the quark distribution in the nucleon. In the Bjorken limit the propagation of the involved quark can be described perturbatively. More recently, factorisation proofs for the DVCS process were derived [22–24], showing that the dominant subprocess, described by the so-called handbag diagram (cf. figure 2), can be factorised. The proof is valid in the region of high momentum transfer Q^2 and low values of $-t$, the square of the four-momentum transfer from the virtual to the real photon.

In electron (or positron) scattering experiments there exists another process that leads to the same final state, namely the Bethe-Heitler process (BH), in which the electron radiates a Bremsstrahlung photon in the Coulomb field of the proton. Hence the contributions of DVCS and BH are entangled in the $e + p \to e' + \gamma + p$ process, thus prohibiting the measurement of the pure DVCS process. The relative contributions of BH and DVCS to the total amplitude depend strongly on the lepton energy. At HERMES energies, the BH contribution is mostly dominant, except at larger values of x and Q^2. This situation is used as an opportunity, since the interference of the two contributions offers a way to access both the real and the imaginary part of the DVCS amplitude. At higher energies, where the DVCS amplitude dominates over the BH amplitude, only the square of the DVCS amplitude can be accessed [25].

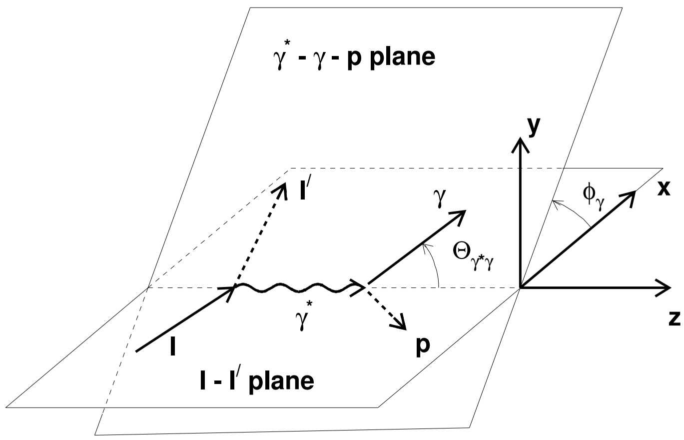

Fig. 3. Schematic visualisation of the angle ϕ between the scattering and the reaction plane.

The process amplitudes describing DVCS, BH and their interference can be expanded into a power series in $1/Q$. They exhibit different characteristics as functions of the azimuthal angle ϕ between the scattering plane and the reaction plane (cf. figure 3), and can be expressed using moments $\langle \cos n\phi \rangle$ and $\langle \sin n\phi \rangle$. These cosine and sine moments are sensitive to the real and imaginary parts of the DVCS helicity amplitudes, respectively. In order to project out the various moments, measurements have to be done with different beam helicity and charge. Under the assumption of the validity of the handbag diagram, each moment has its own characteristic fall-off with $(1/Q)^n$. The first cosine moment is then dominant with a $1/Q$ fall-off, while higher moments fall off with powers of 2 or higher [25]. Even a small lever arm in Q^2 should be sufficient to test the validity of the handbag diagram.

2.2.2 Existing DVCS Analysis at HERMES

A first study of the DVCS process at HERMES has already been carried out. The results are currently being prepared for publication [20]. In this analysis, data taken during the 1996 and 1997 polarised and unpolarised hydrogen running were used to extract the $\langle \sin \phi \rangle$

moment of the observed real-photon production cross section. During these data taking periods, the beam positrons were in the positive (1996 and 1997) and negative (1997 only) helicity states. Since no electron beam was delivered during this period, no beam charge asymmetry could be investigated.

The event selection required that next to the scattered positron a photon was detected as a single untracked cluster in the HERMES calorimeter. Besides the usual data quality cuts, fiducial volume cuts and beam polarisation requirement, cuts were also applied to kinematic variables: $W^2 > 4$ GeV^2, $Q^2 > 1$ GeV^2 and $\nu < 24$ GeV, selecting the hard scattering region. The first step of the analysis was to determine the $\langle \sin\phi \rangle$ moment as a function of the missing mass. A significant non-zero moment was observed for missing mass values below 3 GeV (cf. figure 4).

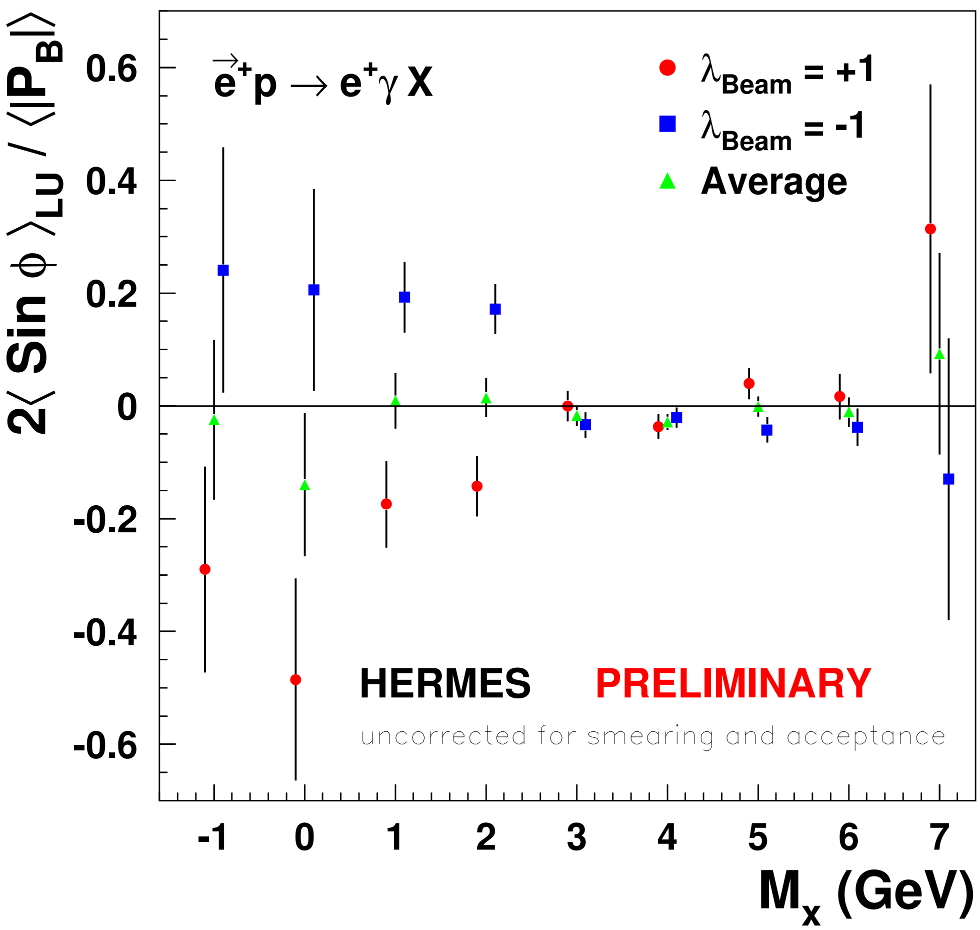

Fig. 4. The $\langle \sin\phi \rangle$ moment of the azimuthal asymmetries vs the missing mass. Circles, squares, and triangles are the results for positive, negative, and helicity averaged results respectively.

The study in its present state still lacks an extensive Monte Carlo simulation that would aid in determining acceptance effects, and that will be necessary to extend the analysis towards the extraction of other $\langle \sin\phi \rangle$ and $\langle \cos\phi \rangle$ moments. In the next analysis step it will also be of importance to extract these moments as functions of Q^2, which is expected to help to verify the dominance of the handbag diagram (factorisation) in the present kinematic region. It would furthermore be helpful to map out the dependences of these moments on x_{Bj} and $-t$. It will also be of importance to implement an improved positioning algorithm for untracked clusters in the calorimeter. This addition will allow the relaxation of the minimum cut on $\theta_{\gamma^*\gamma}$, which corresponds to allowing smaller values of

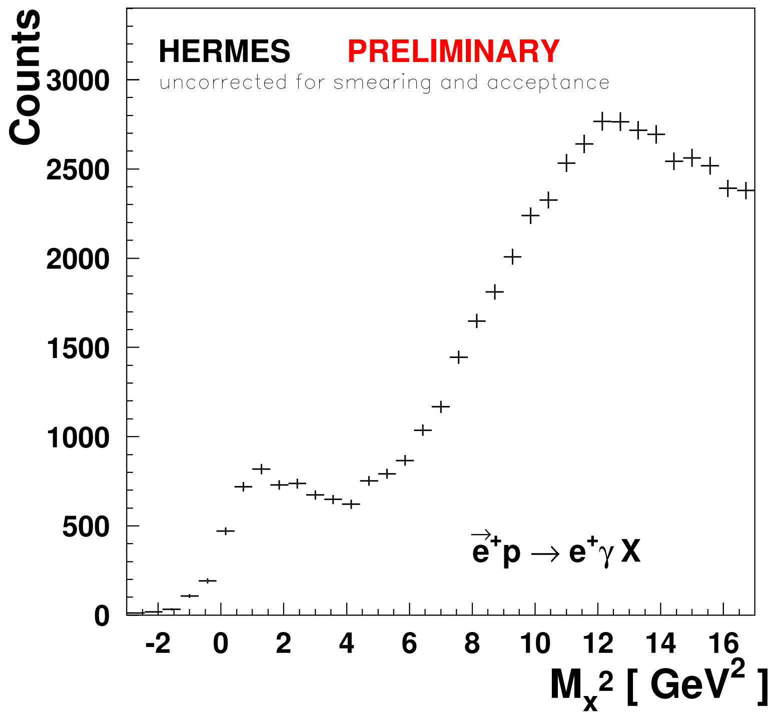

Fig. 5. Square of the missing mass for DVCS candidate events.

$-t$, thus improving the number of DVCS events included in the analysis.

A drawback in the analysis is the relatively poor energy resolution of the calorimeter. Since it is calculated from the four-momenta of the scattered positron and the real photon, the missing mass resolution of typically 0.7 GeV [27](cf. figure 5) is dominated by the energy resolution of the calorimeter. Thus, the missing mass distribution cannot be used to separate exclusive events, where the target proton was left intact, from events where a Δ resonance was produced. There is no experimental indication as to how large the resonant contamination of the DVCS sample is. Detection of the recoil particle will hence be essential both in order to reject non-exclusive events and to gather experimental data on the amount of resonant background to the exclusive process.

2.2.3 Projections for DVCS at HERMES with Recoil Detection

The detection of recoil particles in the measurement of DVCS at HERMES will have two main benefits. The most basic one is the rejection of events in which a resonance was produced. The Δ-resonance will decay into a nucleon and a pion. Since these are produced back-to-back in the rest frame of the Δ, most of the time they will have a transverse momentum component with respect to the direction of the recoil momentum, and thus violate coplanarity with the reaction plane defined by the momenta of the virtual and the real photon. This can be used to minimise the systematic uncertainty due to the unknown resonance contamination of the sample. Furthermore, the distribution of the otherwise rejected resonant events can be studied, and the size of the remaining resonant contamination in the exclusive sample be assessed.

The second benefit of recoil detection for DVCS lies in the reconstruction of the kinematics of the recoil particle. Whereas the determination of the variables Q^2 and x_{Bj}, or W^2 depends solely on the reconstruction of the scattered lepton, $-t$ depends on the reconstruction of the real photon, if the recoil particle is not detected. As a result, the resolution in $-t$, as reconstructed from the real photon's four-momentum is rather poor, approximately 0.25 GeV^2. This variable can alternatively be determined when the four-momentum of the recoiling proton is measured. In this case the resolution in $-t$ depends on the resolution in the proton four-momentum reconstruction. For small values of $-t$ the resolution will be improved by the Recoil Detector by about an order of magnitude (cf. section 3.3.3).

To access the nucleon helicity conserving SPDs H and $\widetilde{H}$ at HERMES with a Recoil Detector an unpolarised proton target is sufficient. In this case two different types of measurement are possible:

(1) Measurements of the beam charge asymmetry with unpolarised leptons:

$$\Delta_C d\sigma^{\mathrm{unp}} \equiv$$
$$d\sigma(e^+p) - d\sigma(e^-p) \sim \cos\phi_\gamma \times \mathrm{Re}\left\{F_1\mathcal{H}_1 + \frac{x_B}{2-x_B}(F_1+F_2)\widetilde{\mathcal{H}}_1 - \frac{\Delta^2}{4M^2}F_2\mathcal{E}_1\right\} \quad (6)$$

The asymmetry allows to access the real parts of the DVCS amplitudes $\mathcal{H}_1$, $\widetilde{\mathcal{H}}_1$, and $\mathcal{E}_1$.

(2) Measurements of the beam spin asymmetry with polarised positron beam and unpolarised target:

$$\Delta d\sigma \equiv$$
$$d\sigma(\overrightarrow{e^+}p) - d\sigma(\overleftarrow{e^+}p) \sim \sin\phi_\gamma \times \mathrm{Im}\left\{F_1\mathcal{H}_1 + \frac{x_B}{2-x_B}(F_1+F_2)\widetilde{\mathcal{H}}_1 - \frac{\Delta^2}{4M^2}F_2\mathcal{E}_1\right\} \quad (7)$$

This asymmetry allows an access to the imaginary parts of the same amplitudes. Note that in both cases $\mathcal{E}_1$ appears suppressed and $\widetilde{\mathcal{E}}_1$ cannot be accessed at all.

The imaginary and real parts of the DVCS amplitudes are related to the SPDs:

$$\begin{aligned}
\mathrm{Im}\,\mathcal{H}_1 &= -\pi\sum_q e_q^2\Big(H(\xi,\xi,\Delta^2) - H(-\xi,\xi,\Delta^2)\Big)\\
\mathrm{Im}\,\widetilde{\mathcal{H}}_1 &= -\pi\sum_q e_q^2\Big(\widetilde{H}(\xi,\xi,\Delta^2) + \widetilde{H}(-\xi,\xi,\Delta^2)\Big)\\
\mathrm{Re}\,\mathcal{H}_1 &= \sum_q e_q^2\Big[P\int_{-1}^{+1} H(x,\xi,\Delta^2)\left(\frac{1}{x-\xi}+\frac{1}{x+\xi}\right)dx\Big]\\
\mathrm{Re}\,\widetilde{\mathcal{H}}_1 &= \sum_q e_q^2\Big[P\int_{-1}^{+1} \widetilde{H}(x,\xi,\Delta^2)\left(\frac{1}{x-\xi}-\frac{1}{x+\xi}\right)dx\Big]
\end{aligned} \quad (8)$$

where P denotes Cauchy's principal value. Analogous expressions are valid for the DVCS amplitudes $\mathcal{E}_1$ and $\widetilde{\mathcal{E}}_1$.

For the projection of the expected statistical accuracy of DVCS measurements at HERMES with a Recoil Detector an approach from [28] was adopted. The authors calculated the amplitudes of the DVCS, Bethe-Heitler and interference terms at twist-two level for different kinds of polarised and unpolarised initial particles. To model the SPDs, a simple ansatz proposed in paper [26] was adopted. For example, H was taken as the product of a form factor and a quark distribution function, neglecting any ξ dependence, which yields :

$$\begin{aligned} H^{u/p}(x,\xi,\Delta^2) &= u(x)\, F_1^{u/p}(\Delta^2)/2 \\ H^{d/p}(x,\xi,\Delta^2) &= d(x)\, F_1^{d/p}(\Delta^2) \\ H^{s/p}(x,\xi,\Delta^2) &= 0 \end{aligned} \tag{9}$$

where $u(x)$ and $d(x)$ are the unpolarised quark distributions. The elastic form factors for one quark flavor have to be related to the physical ones. Restricting to the u, d quark flavors, the Dirac and Pauli form factors are expressed as

$$F_{1(2)}^{u/p} = 2F_{1(2)}^{p} + F_{1(2)}^{n}\ , \qquad F_{1(2)}^{d/p} = 2F_{1(2)}^{n} + F_{1(2)}^{p}\ , \tag{10}$$

where $F_{1(2)}^{p}$ and $F_{1(2)}^{n}$ are the proton and neutron electromagnetic form factors respectively.

The projections of statistical accuracy for measurements of the beam charge (6) and beam helicity (7) asymmetries at HERMES were calculated for the integrated luminosity value of 2 fb^{-1} (cf. section 2.7) [29]. The HERMES acceptance for the detection of the scattered electron, the real gamma and the recoil proton has been taken into account. The following kinematic cuts were applied: $E_e > 3.5$ GeV, $E_\gamma > 1$ GeV, $P_p > 0.2$ GeV, $W^2 > 4$ GeV^2, $Q^2 > 1$ GeV^2, and $15 < \Theta_{\gamma\gamma^*} < 70$ mrad. Projections of the statistical accuracy for measurements of the beam helicity asymmetry are presented in fig. 6 as a function of the azimuthal angle ϕ_γ (left panel) and as a function of x for different bins in $-t$ (right panel). For comparison the data points extracted from 1996/97 HERMES data are shown as well [20].

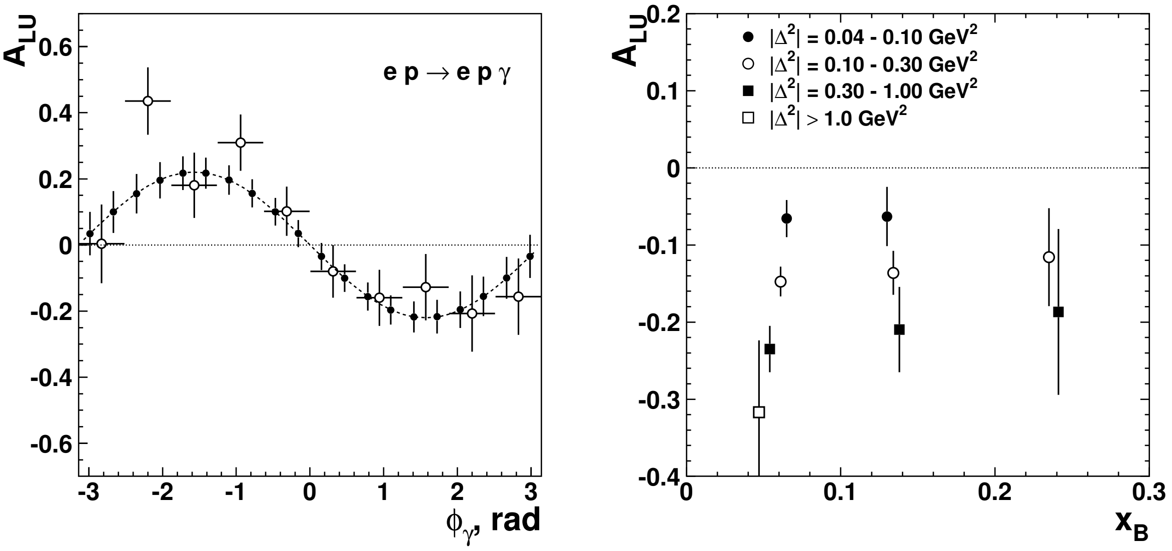

Fig. 6. Left: Projection of the global statistical accuracy of the beam helicity asymmetry (7) as a function of the azimuthal angle, ϕ_γ, between the scattering and production planes. Projections are based on 2 fb^{-1}, in comparison to the 1996/97 data representing 0.13 fb^{-1}. Right: Projection for the x-dependence of the beam helicity asymmetry for different bins in $-t = \Delta^2$.

The projections for the statistical accuracy of the beam charge asymmetry are presented in fig. 7. The left figure shows the ϕ_γ-dependence, while the right figure shows a significant

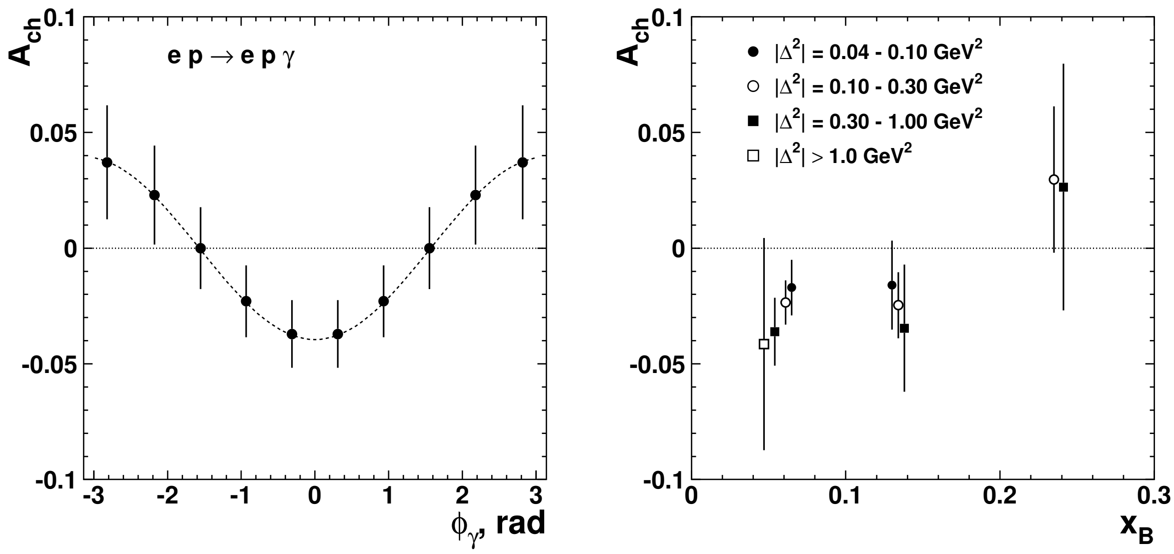

Fig. 7. Left: Projection of the statistical accuracy of the beam charge asymmetry (6) as a function of the azimuthal angle, ϕ_γ, between the scattering and production planes. Right: Projection for the x-dependence of the beam charge asymmetry for different values of $-t = \Delta^2$. Based on 2 fb^{-1}.

x- and t-dependence including a sign-change at about $x = 0.2$. Note that this dependence of the asymmetry on x is mainly a consequence of the SPD model adopted for the calculations. It may be concluded that a measurement of hard exclusive real gamma production will allow separate access to the real and imaginary parts of the same DVCS amplitude combinations from which constraints for the SPD's modeling will be derived.

2.3 Exclusive Production of Vector Mesons

Electroproduction of neutral vector mesons at intermediate energies is an important research topic of the HERMES Experiment. So far the production of ρ^0 [30], ω [31], ϕ [32], and J/ψ [33] has been studied. Several HERMES papers have already been published on ρ-production [17,18,34]. All of these diffractive processes involve the exchange of some neutral object(s) between the virtual photon and the target nucleon, whereby the former is dissociating into a vector meson carrying essentially the quantum numbers of the photon.

Theoretically, the interpretation of the exchanged neutral object(s) depends on the values of W and Q^2 at which the process occurs. At low values of Q^2 the Vector Meson Dominance model can provide a phenomenological description of the world data by assuming Pomeron exchange between the virtual photon and the nucleon, where the former fluctuates into a vector meson. At higher values of W and moderate Q^2 pQCD-models based on two-gluon-exchange mechanisms are quite successful. However, they are not able to describe HERMES data at lower values of W, although the model given in [35] might still be applicable. This is especially seen for light vector mesons like the ρ^0. Only if an additional contribution from quark exchange is included [26], the measured data can be explained (fig. 8). Therefore such an SPD-based approach appears promising in interpreting the HERMES data. Note that in vector meson production only the unpolarised SPDs are involved.

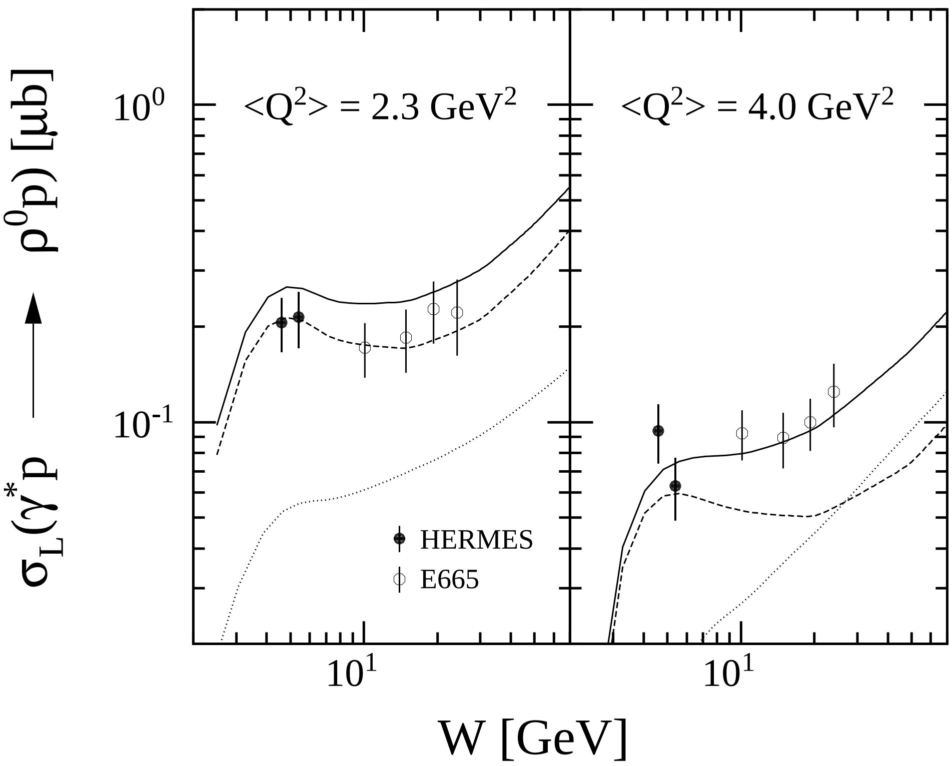

Fig. 8. Longitudinal part of the exclusive ρ^0-photoproduction cross-section as a function of W at $Q^2 = 2.3$ and $Q^2 = 4.0$ GeV^2 [17]. Data points are from HERMES and E665 (semi-exclusive). Model predictions according to Vanderhaeghen et al.: SPD-based quark exchange mechanism (dashed), two-gluon-exchange (dotted) and sum (solid).

On the other hand, such a comparison is only possible, if purely exclusive rho-production is observed. As the missing mass resolution of HERMES exceeds one pion mass in all exclusive processes, this condition is not trivially fulfilled. While a number of methods have been developed to subtract DIS background [33], a substantial contribution is expected from double-dissociative diffraction, in which the nucleon breaks up into a multi particle state with low invariant mass. A parameterisation derived from pp-scattering [36] suggests that the invariant mass distribution of the nucleon fragments peaks around 1.3 GeV, such that in most cases a nucleon and a pion are produced. The percentage of these events within the current ρ-sample is estimated as 7.5 ± 2.0 %, while for ω-mesons 13.0 ± 3.4 % is expected [31]. However, some model predictions are much higher, up to 30% [37].

In a similar way as described above for the DVCS case, the Recoil Detector will be able to remove a major part of the non-exclusive background. This will allow for a cleaner determination of spin density matrix elements; the combination of the polarised beam with the unpolarised target will especially enable the study of polarisation dependent quantities like $Tr(r^8)$ [34]. The improved exclusivity level of the events will also lead to new constraints on SPDs. It is worth noting that SPD-based models also provide predictions for the exclusive production of ρ^+-mesons which is only possible via quark exchange. First ρ^+ signals have already been studied [31], although still a large background is present.

The study of the effect of a Recoil Detector on the detection of vector mesons has so far been restricted to ρ-mesons. This can be generalised because the kinematics of exclusive ρ, ω, and ϕ-production is similar due to their similar masses. Only for J/ψ-production a large difference is expected, but the J/ψ can anyway not be produced via quark exchange.

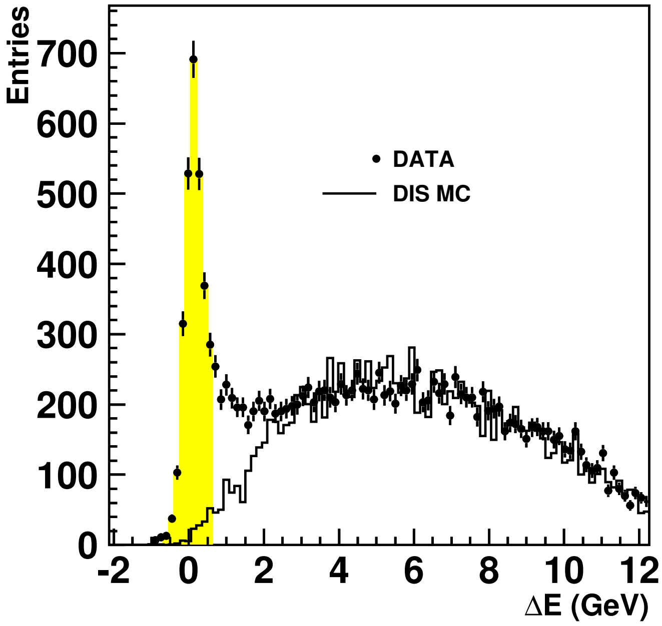

Fig. 9. Missing energy spectrum for rho-production at HERMES. Exclusive region below $\Delta E = 0.6$ GeV is shaded. DIS-background from Monte-Carlo.

The ρ^0-meson will be an important channel to study with the Recoil Detector at HERMES, because besides the above arguments it gives the cleanest signal via its only and self-analyzing decay channel to two charged pions and at HERMES it is detected with the highest rate of all exclusive processes (about 930 exclusive events per 10^6 DIS-events in the polarised year 2000-sample [38]). Presently most of the ρ-analysis done at HERMES uses the method of missing energy in order to ensure exclusivity. In figure 9 a clear signal of the exclusive rho-production is seen at a missing energy of zero, reconstructed from events with two oppositely charged pions. Conventionally a restrictive cut at a missing energy of $\Delta E = 0.6$ GeV is applied, which removes most of the DIS-background. The background suppression through the information from the recoil detector will make a more relaxed cut possible, thus increasing the statistics.

Double-dissociative diffractive background is also present in the missing energy range below 2 GeV. A simple Monte Carlo generation based on the parameterisation given in [36] shows that the recoil detector will be very effective in reducing this background due to the well-known ρ-kinematics. While keeping 80% of the exclusive events, the double-dissociative background within the cut region may be reduced to less than 10%.

2.4 Exclusive Production of Pseudoscalar Mesons

Hard exclusive electroproduction of pseudoscalar mesons has been described in terms of SPDs since factorisation has been proved for longitudinal photons [39]. In the pion electroproduction process, the polarised SPDs are involved and therefore this reaction is directly related to the spin physics that is generally studied in polarised DIS.

The hard longitudinal electroproduction of charged pions receives contributions from two production mechanisms: the photon interaction with one quark that combines via hard gluon exchange with a second quark from the target, and the absorption of a photon by a pion in the meson cloud of the nucleon (the so-called pion-pole contribution). Both mechanisms have been described in the pQCD factorisation scheme [40].

While at intermediate $-t$ and small x both terms may contribute and interfere, the pion pole contribution is expected to be dominant in the small $-t$ region and at large x. In this region the determination of the space-like pion form factor will in principle be possible once a reliable parameterisation of the contribution from transverse photons becomes available. This contribution is in any case expected to be small for the HERMES kinematics. Presently the space-like pion form factor is almost unknown for Q^2 larger than 2 GeV^2 and the theoretical predictions strongly differ from one another [41].

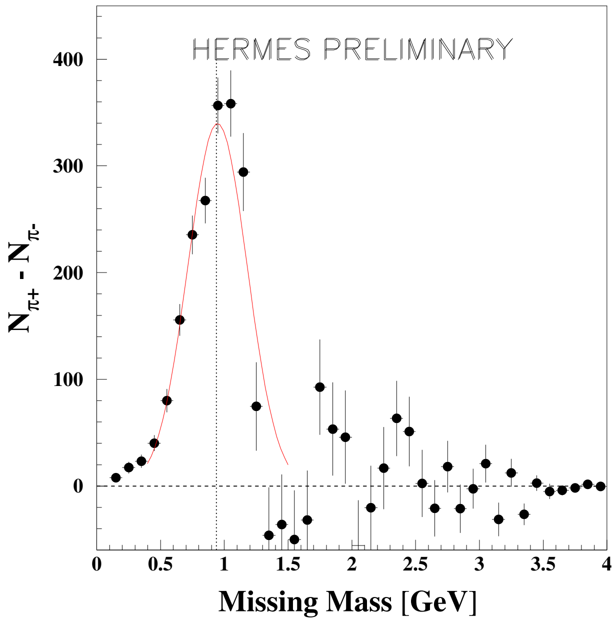

Fig. 10. Missing mass distribution for exclusive π^+ events obtained after subtraction of the π^- distribution.

HERMES already has acquired some expertise in exclusive pion production through the recently performed first measurement of exclusive π^+ production on a pure polarised hydrogen target,at $Q^2 > 1$ GeV^2. The exclusive process is selected by detecting the leading π^+ and assuming the π^- distribution being a good estimate of the background in the missing mass region of the recoiling nucleon. A clear peak in the missing mass distribution (cf. figure 10) has been found with position and width in agreement with the expectation. The missing mass resolution is about 0.25 GeV for the exclusive events. The non-exclusive background contamination, which depends on the missing mass cut, is of the order of 20%. The kinematic distributions of the events (vs. Q^2, x, $-t$) agree well with the expectations resulting from a Monte Carlo simulation based on an exclusive pion generator which includes the pion pole contribution. A careful investigation of the efficiency and acceptance for this process in under study to provide the absolute value of the total cross section.

In addition, the $\langle \sin\phi \rangle$ moments of the single spin asymmetries (SSA) of this process with respect to the longitudinal target spin have been measured. Here ϕ is the azimuthal angle of the pion with respect to the lepton scattering plane, around the virtual photon direction. A dramatic sign change for the π^+ SSA is observed in the exclusive limit $z \to 1$ (cf. figure 11). This behavior may arise from the interference between the pole and non-pole contributions as predicted for the transverse target case [42] where a SSA of the order of unity is expected.

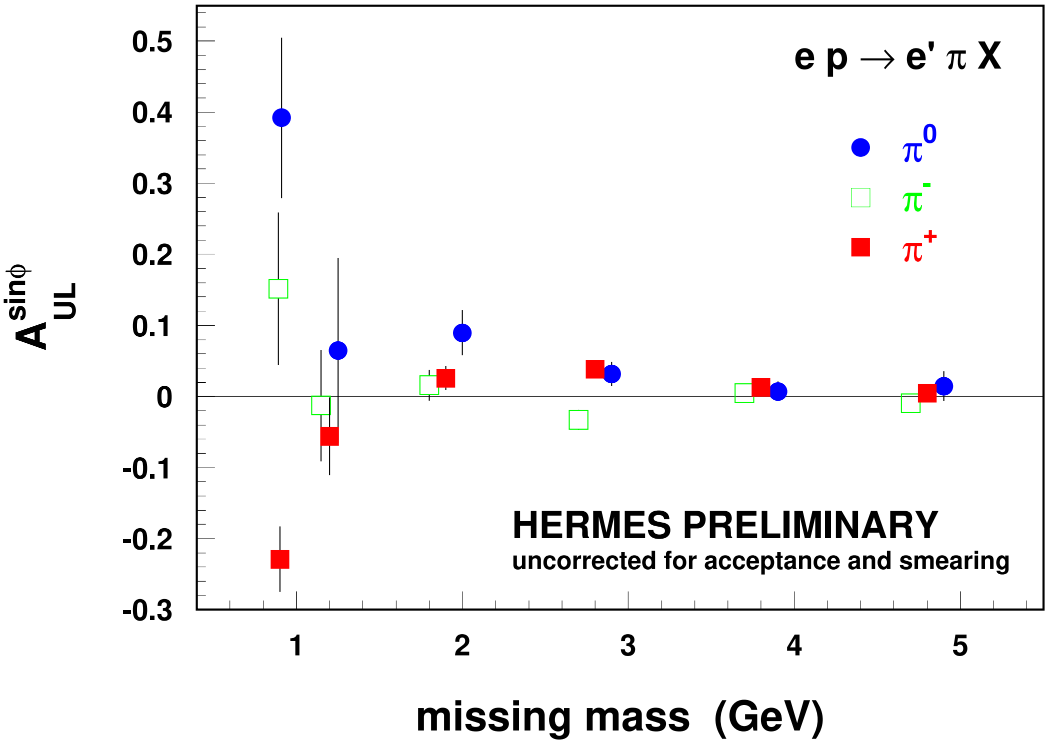

Fig. 11. Single Spin Azimuthal Asymmetries for pions as a function of the missing mass. Unpolarised beam and longitudinally polarised target.

The distribution of the recoiling neutron in the reaction $ep \to \pi^+ n$ is similar to that of the recoiling proton distribution for DVCS events shown in figure 13. In the given geometry of the HERMES spectrometer a neutron detector, that typically would be based on the time-of-flight technique, is not feasible. The main background consists of reactions with an intermediate Δ^0 resonance that in turn decays into $p\pi^-$ or $n\pi^0$. Thus the exclusivity of a π^+-production event can be established by the absence of a signal from either a recoil proton or a π^- or π^0 from a Δ^0-decay. The Recoil Detector will therefore in this case be used as a veto counter.

The proposed Recoil Detector can be used even more effectively for the hard exclusive electroproduction of neutral pseudoscalar mesons (like π^0, η and η') where the recoil proton can be detected. These processes can provide a direct access to the polarised SPDs without the pole term present in the charged pion case. In addition, it has been argued that the study of the ratios of exclusive $\pi^0 : \eta : \eta'$ yields from proton and deuteron targets can give a way to probe the physics of spontaneous chiral symmetry breaking [43]. Strong variations of the above yields are expected when going from the semi-inclusive fragmentation kinematics to exclusive processes.

Due to the missing mass resolution of the HERMES forward spectrometer (about 0.4 GeV for exclusive π^0) and to the low cross sections of these processes, the HERMES capabilities to study the exclusive neutral pseudoscalar meson electroproduction are currently quite limited. Additionally, no experimental information on the non-exclusive background is available, as in the exclusive π^+ case. High luminosity data together with the detection of the recoiling protons of the process $ep \to e\pi^0(\eta, \eta')p$ will strongly improve the potential of such a measurement. Due to the similar kinematics and similar missing mass resolution, exclusive π^0 data will be improved by a recoil-detector in much the same way as DVCS data.

In addition to the exclusive single pseudoscalar meson electroproduction, it has been suggested that the study of the hard exclusive electroproduction of pion pairs ($\pi^+\pi^-$ and $\pi^0\pi^0$) will provide a novel technique to study the structure of mesons and the gluon content of the isoscalar $\pi\pi$ state [44]. The measurement of these processes will benefit similarly from the detection of the recoiling proton.

2.5 Λ Production

An exciting additional physics topic is the measurement of Λ-polarisation in the target fragmentation region. The self-analyzing (parity violating) decay $\Lambda \to p+\pi^-$ ($\bar{\Lambda} \to \bar{p}+\pi^+$) provides an opportunity to measure the polarisation of Λ ($\bar{\Lambda}$) hyperons. The measurement of the spin transfer from the longitudinally polarised electron (positron) beam to the Λs produced in Deep Inelastic Scattering in the current fragmentation region ($x_f > 0$) is an important experimental test of the spin structure of the Λ [45,46], provided that the fractional energy z transfered to the Λ hyperon is high enough (close to 1).

As it has been shown in ref. [47], the polarisation transfer in the target fragmentation region ($x_f < 0$) is sensitive to the target spin structure, in particular to the strange quark spin content. If a beam electron has positive helicity, it removes from the nucleon also a quark of positive helicity, typically a u-quark (u-quark dominance). In order to form the Λ a $s\bar{s}$ pair must be produced. Assuming that the $s\bar{s}$ pair is produced in the $^3P_0$ vacuum state [47], the quark spins are parallel and they can be either parallel or antiparallel to the u quark spin. In order to measure the polarisation of the s quark in the remnant the produced Λ can then be used as a 'polarimeter', given the fact that the polarisation of an s-quark in the Λ is quite high, ranging from 60 to 100 % in different models [46].

Until now the longitudinal spin transfer to the Λ has been measured at HERMES only in the current fragmentation region ($x_f > 0$). These measurements used the polarised electron/positron beam and an unpolarised gas target. Preliminary results are reported in references [48,49]. In figure 12 they are shown together with results from NOMAD [50] (ν beam) and WA59 [51] at CERN ($\bar{\nu}$ beam). Although in both neutrino experiments the polarisation transfer coefficient in the target fragmentation region has the same (negative) sign their results disagree significantly. A HERMES measurement could help to resolve this disagreement.

The direction of the polarisation in the HERA e-ring can be reversed. Combining data from appropriate run periods allows the extraction of the Λ polarisation without any Monte Carlo simulation of the spectrometer acceptance. The result is model independent. With this experimental advantage it would be particularly interesting to access also the kinematic domain of target fragmentation ($x_f < 0$) where about 70% of the Λs in HERMES are produced. Together with the Lambda-Wheels, the Recoil Detector will provide a practically complete coverage for pions from Λ decays. As it has been seen in Monte Carlo studies (cf. ref. [1]), it is sufficient for Λ identification to have only track information for the pion if the proton momentum is measured. The gain in statistics due to the Recoil Detector is estimated to be 1.8. In addition the acceptance becomes practically uniform, i.e. $\cos\theta \simeq$ const, where θ is the decay angle in the Λ rest frame.

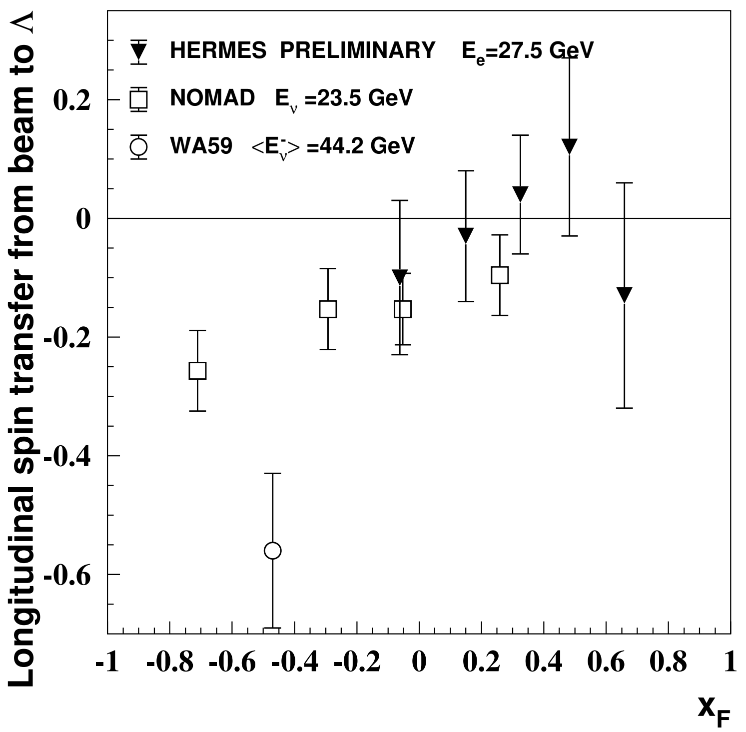

Fig. 12. Recent results on longitudinal spin transfer to the Λ.

2.6 Other Physics

The physics topics described in section 2.3 of the original Recoil Detector proposal [1] can in principle also be addressed with the Large Acceptance Recoil Detector, albeit with a slightly higher low-momentum cut-off. This includes the measurement of F_2^n/F_2^p and a study of the possible origin of the EMC effect.

2.7 Expected Luminosity

Based on the performance of the HERA accelerator and the HERMES spectrometer in 2000, the annual integrated luminosity after the installation of the Recoil Detector can be estimated to about 2 fb^{-1}. This is based on the assumption of 200 days of HERA operation with on average 1.5 HERA fills per day, an average beam current of 25 mA during normal operation and 10 mA during end-of-fill running. The density of the unpolarised HERMES target is assumed to be $1 \cdot 10^{15}$ nucleons/cm^2 during normal operation and $1 \cdot 10^{16}$ nucleons/cm^2 during end-of-fill running. The resulting 2 fb^{-1} per year correspond to about 90 million DIS events or, including the overall acceptance of the Recoil Detector for DVCS of 89%, to about 80,000 reconstructed DVCS/BH events. Running for one years in this configuration would increase the DVCS/BH statistics by a factor of about 15 compared to the combined statistics from 1996/97 or the statistics from 2000.

2.8 Competing Experiments

Hard exclusive leptoproduction experiments for the study of SPDs are being prepared at both Jefferson Lab and COMPASS. An overview of the planned experiments is shown in table 1.

Experiment	Process(es)	$\mathcal{L}$ [$\mathrm{cm}^{-2}\mathrm{s}^{-1}$]	x	Q^2 [GeV^2]
CLAS (Hall B) JLAB E 99-105	$e^- p \to e^-(\rho,\omega)p$	10^{34}	0.1-0.45	1 - 4.5
Hall A JLAB E 00-110	$e^- p \to e^- \gamma p$	10^{37}	0.3-0.4	1.5 - 2.5
COMPASS	$\mu^+ p \to \mu^+(\gamma,\pi)p$	$1.5 \cdot 10^{32}$	0.05-0.4	2 - 5
HERMES	$e^\pm p \to e^\pm \gamma p$ $e^\pm p \to e^\pm(\rho,\omega,\phi)p$ $e^\pm p \to e^\pm \pi p$	$2.0 \cdot 10^{32}$	0.05-0.3	1 - 5

Table 1
Main features of exclusive lepton scattering experiments in the world. The luminosity is given in units of $\mathrm{cm}^{-2}\mathrm{s}^{-1}$.

At Jefferson Lab one approved experiment in Hall B will study exclusive ρ and ω production [52]. This experiment covers the kinematic range of $0.1 < x < 0.45$ and $1 < Q^2 < 4.5$ GeV^2. While the expected integrated luminosity is almost one order of magnitude higher than at HERMES, the smaller cross section at 6 GeV will lead to about comparable statistics.

Another experiment at Jefferson Lab in Hall A has recently been conditionally approved [53]. This experiment aims at the measurement of the DVCS/BH interference terms in much the same way as HERMES and has a significantly higher luminosity. However, at 6 GeV the cross section is almost completely dominated by BH and compared to HERMES kinematics the interference term is suppressed by 2-3 orders of magnitude. Hence some of the advantage in luminosity is lost again. The experiment has only a very limited kinematic range in x and Q^2. Measurements of beam charge asymmetries are not possible at Jefferson Lab, as only an electron beam is available.

At the 200 GeV muon energy of the COMPASS experiment DVCS clearly dominates over BH. There is a proposal for an upgrade of the COMPASS experiment with a Recoil Detector [54] to measure DVCS on a proton target. The expected luminosity is comparable to the HERMES luminosity during normal operation. In principle also measurements with negative muons would be possible at COMPASS, albeit with significantly reduced luminosity. However, regular data taking has not yet been started at COMPASS.

The proposed measurements at HERMES with a Recoil Detector are building on the already existing HERMES measurements of exclusive ρ and π production and DVCS. Their strength lies in the completeness of the approach: Measuring a large variety of exclusive processes over an extended kinematic range with the same detector. Furthermore, HERMES currently is the only experiment that will be able to measure both beam spin and beam charge asymmetries, which e.g. is the only way to separately measure the real and imaginary parts of the DVCS amplitudes.

3 Recoil Detector Design

3.1 Design Requirements

The energy and position resolution of the HERMES spectrometer is not sufficient to ensure the exclusivity of any given event. This can e.g. be seen in the missing mass resolution for DVCS events (770 MeV) shown in figure 5.

The purpose of the Recoil Detector is to measure all necessary observables for the involved particles to ensure the exclusivity of a given event sample. To this end it must be able to

- identify the recoil proton through a combination of tracking, charge determination and separation from possible π^+ background,
- measure the momentum of the recoil proton in the range from 100 to 1200 MeV/c in the relevant angular region ($0.2 < \theta < 1.35$, i.e. $10^\circ < \theta < 80^\circ$).
- detect and identify charged pions from associated Δ-production,
- detect π^0s from Δ-decays to help reduce the background from associated Δ-production and
- be as hermetic as possible.

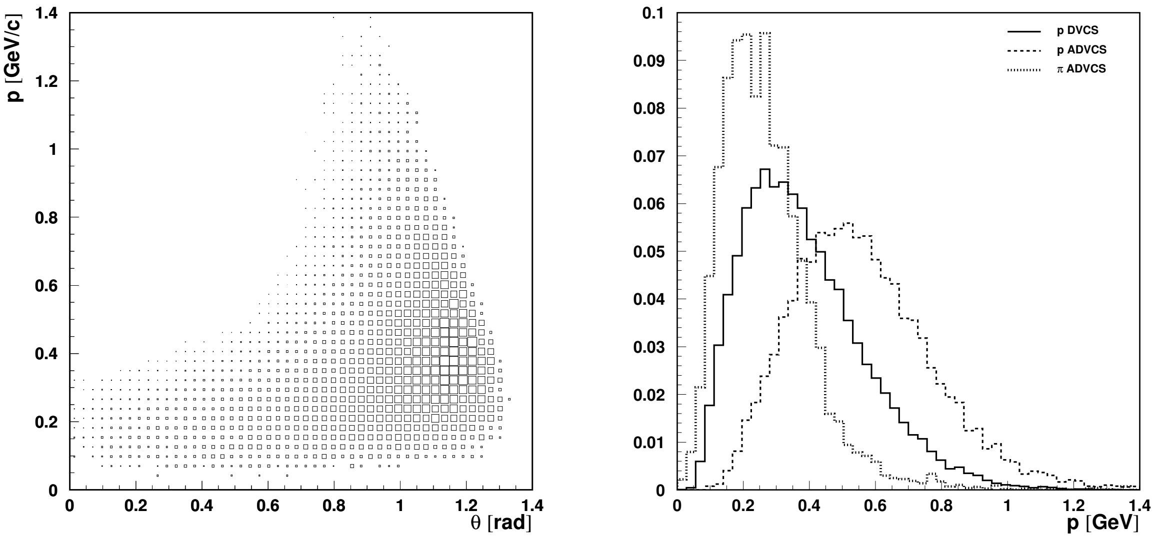

Fig. 13. Kinematics of the particles the Recoil Detector should detect. The left figure shows the distribution of recoil protons from DVCS events in momentum p and polar angle θ (relative to the z-axis defined by the beam direction). The right figure shows the normalised momentum distributions for DVCS recoil protons in comparison to protons and pions from intermediate Δ decays (ADVCS). (The spectra have been normalised to unity.)

Figure 13 illustrates the kinematics of the particles the Recoil Detector should detect. The left side shows the distribution of DVCS recoil protons in polar angle θ and momentum

p. The bulk of the statistics is located at angles between 0.9 and 1.3 rad and momenta between 200 and 600 MeV/c. This figure is very similar also for the other hard exclusive processes. The right side of figure 13 shows normalised momentum spectra for recoil protons from DVCS and so-called associated DVCS (ADVCS), i.e. background processes with intermediate Δ^+, as well as for pions from ADVCS (π^+ from $\Delta^+ \to n\pi^+$). Hardly any pions can be expected at momenta above about 600 MeV/c. This defines the momentum range for which a pion/proton particle identification is required.

3.2 Conceptual Detector Design

Driven by the short time span available for design, construction and testing of the HERMES Recoil Detector, the general guideline for the design is to keep everything simple, reliable and to use only standard 'off-the-shelves' parts wherever possible. The R&D phase, usually typical for the design of a new detector, will in this way be reduced to a minimum, saving both time and manpower resources.

The Large Acceptance Recoil Detector consists of three active detector parts: A silicon detector around the target cell inside the beam vacuum, a scintillating fibre tracker in a longitudinal magnetic field and a layer of scintillator strips (or pads) that uses the return yoke a preshower material.

The inner part of the Large Acceptance Recoil Detector is, as in the original Recoil Detector proposal, a silicon detector. Its design starts from the assumption that TIGRE silicon detectors from Micron Semiconductors will be used. They have a thickness of 300 μm, double-sided readout and 128 channels on each side. Together with the dimensions of 10×10 cm^2 this corresponds to a pitch of 0.78 mm. Two detectors each are chained together to form 10×20 cm^2 units from which the silicon tracker is constructed. As can be seen in the top part of figure 16, four such units in a 'diamond structure' around the target cell form the first silicon layer, four further units form the second layer with a distance of 1.5 cm between both layers. The given size of the silicon detectors and the acceptance requirements lead to a reduced length of the target cell of 15 cm. The given size of the detectors also leads to the four gaps in the silicon detector acceptance and to the required diameter of the beam pipe of 19 cm. The readout of the silicon detectors will be located upstream and the holding structure (indicated on both sides in figure 16 top) will also be supported from the upstream flange. The aluminium beam pipe can therefore be rather thin, about 1.0 to 1.1 mm [55].

A significant background arises from electrons from Møller scattering. This has already been studied in the original Recoil Detector proposal [1]. For the modified geometry of the Large Acceptance Recoil Detector a longitudinal magnetic field of about 0.7 T ensures that virtually no primary Møller electrons can hit even the inner silicon layer. This is illustrated in figure 14. Therefore 0.7 T has been taken as the minimum value for the longitudinal magnetic field. As will be seen in the following section 3.3, there are good reasons to use a somewhat larger magnetic field of about 1.0 T. It will still have to be studied if this leaves the HERA beam and the HERMES forward spectrometer unaffected. The magnet will likely have to be a superconducting one with an iron return yoke that is several cm thick.

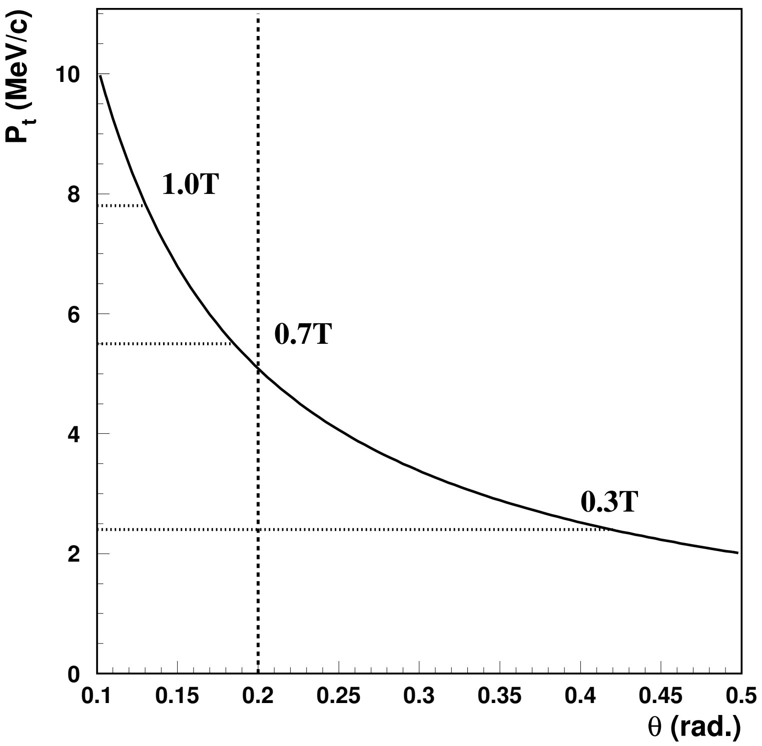

Fig. 14. Relation between the transverse momentum of the Møller electrons and their polar angle θ. The dashed line marks the lower limit of the acceptance for the inner layer of the silicon detector at 0.2 rad. For a field of 0.7 T Møller electrons with transverse momenta p_t below 5.5 MeV will not reach the silicon detector.

The silicon detectors will be read out using the APC128 chip [56], which has a limited dynamic range of about 15 [57]. The largest signals expected in the inner silicon detector are about 8 MeV, which leads to a detection threshold at about 0.5 MeV that corresponds to 3-4 MIPs. This in turn corresponds to a high-momentum cut-off for the silicon detector at about 500 MeV. Protons with higher momenta will not be detected by the silicon tracker. The low-momentum cut-off of the acceptance of the silicon tracker is given by the absorption of particles in the target cell walls and in the first silicon layer. Requiring two full space points, i.e. signals from both silicon layers, this cut-off is at about 110 MeV/c. The value was determined using a Monte Carlo simulation of the detector.

An outer scintillating fibre (SciFi) tracker together with the longitudinal magnetic field is the perfect complement to the inner silicon tracker. The scintillating fibre tracker follows the basic design of a fibre tracker study for a future linear collider experiment as outlined in [58]. It consists of two scintillating fibre detectors with inner diameters of 19 and 32 cm, respectively. Each fibre detector consists of 8 layers of scintillating fibres, the first 4 parallel to the z-axis (the beam) and the second 4 under a small stereo angle (about 10°). Four fibres, one from each layer, forming a 'road' along the radius, will be combined into one readout channel, in a similar fashion as described in [59]. With fibre diameters of 0.5 mm for the inner SciFi detector and 1.0 mm for the outer SciFi detector there will be a total of 17600 fibres, corresponding to 4400 readout channels. The readout will likely use multi-channel photomultiplier tubes (PMTs), e.g. 64 channel PMTs from Hamamatsu. The low-momentum cut-off for the SciFi tracker (requiring two full space points) was found by Monte Carlo simulation to be around 260 MeV/c.

The resolution of the SciFi detector is dominated by the effects of multiple scattering. This is illustrated in figure 15. For this study a sample of DVCS MC events without magnetic field has been used to provide straight proton tracks. The left plot of figure 15 shows the effect of multiple scattering in terms of the difference between the azimuthal angle ϕ_2 at the outer SciFi detector and the original angle ϕ_0. The plot integrates over all momenta and the center of the distribution has a width of 4.2 mrad. The right plot shows the momentum dependence of the multiple scattering effects. Shown here is the RMS value $\Delta\phi$ of the distribution of $\phi_2 - \phi_0$ as a function of the recoil proton momentum. The two lines indicate the expected contribution to the resolution that results from the fibre diameter, estimated as $d/\sqrt{12}$ for the fibre diameter d. For the outer SciFi detector (SciFi2) the contribution from multiple scattering is larger than the expected contribution from the fibre diameter over the entire momentum range, for the inner SciFi detector this is true up to about 0.75 GeV/c. The figure indicates that no significant improvement in ϕ-resolution, and as a result in momentum resolution, could be expected from smaller fibre diameters.

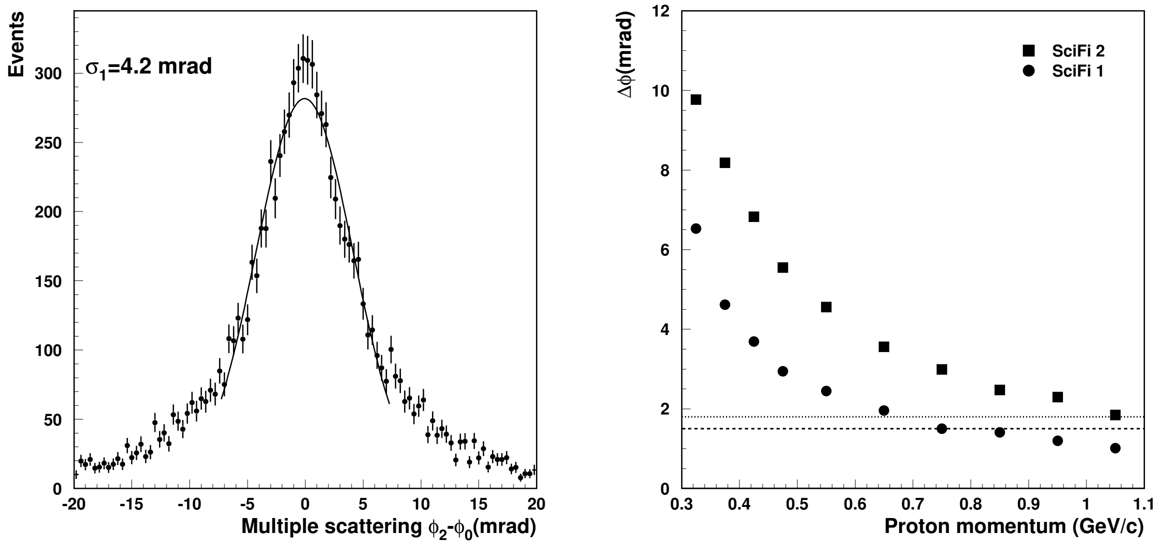

Fig. 15. Multiple scattering effects in the SciFi detector. Left: Difference between the azimuthal angle ϕ_2 at SciFi2 and the original angle ϕ_0. Right: RMS value $\Delta\phi$ of the distribution of $\phi_2 - \phi_0$ as a function of the recoil proton momentum. The two lines indicate the expected contribution to the resolution that results from the fibre diameter, estimated as $d/\sqrt{12}$ for the fibre diameter d (dashed: SciFi1, dotted SciFi 2).

The Recoil Detector is completed by a π^0-detector that uses the return yoke of the magnet as preshower material. The π^0-detector itself will consist of scintillator strips or pads and (as much as possible) use the same readout technology as the SciFi tracker. In addition it may also serve as time-of-flight detector to improve the π/p-separation.

A schematic overview of the Recoil Detector can be seen in figure 16. The upper drawing shows a cross section through the detector, while the lower drawing shows a top view of the detector. The dashed line in the schematic top view indicates the acceptance of the forward HERMES spectrometer. The gap between the SciFi detector and the Λ-wheels (z=34-45 cm) is necessary to accomodate flanges that are not shown in this schematic drawing.

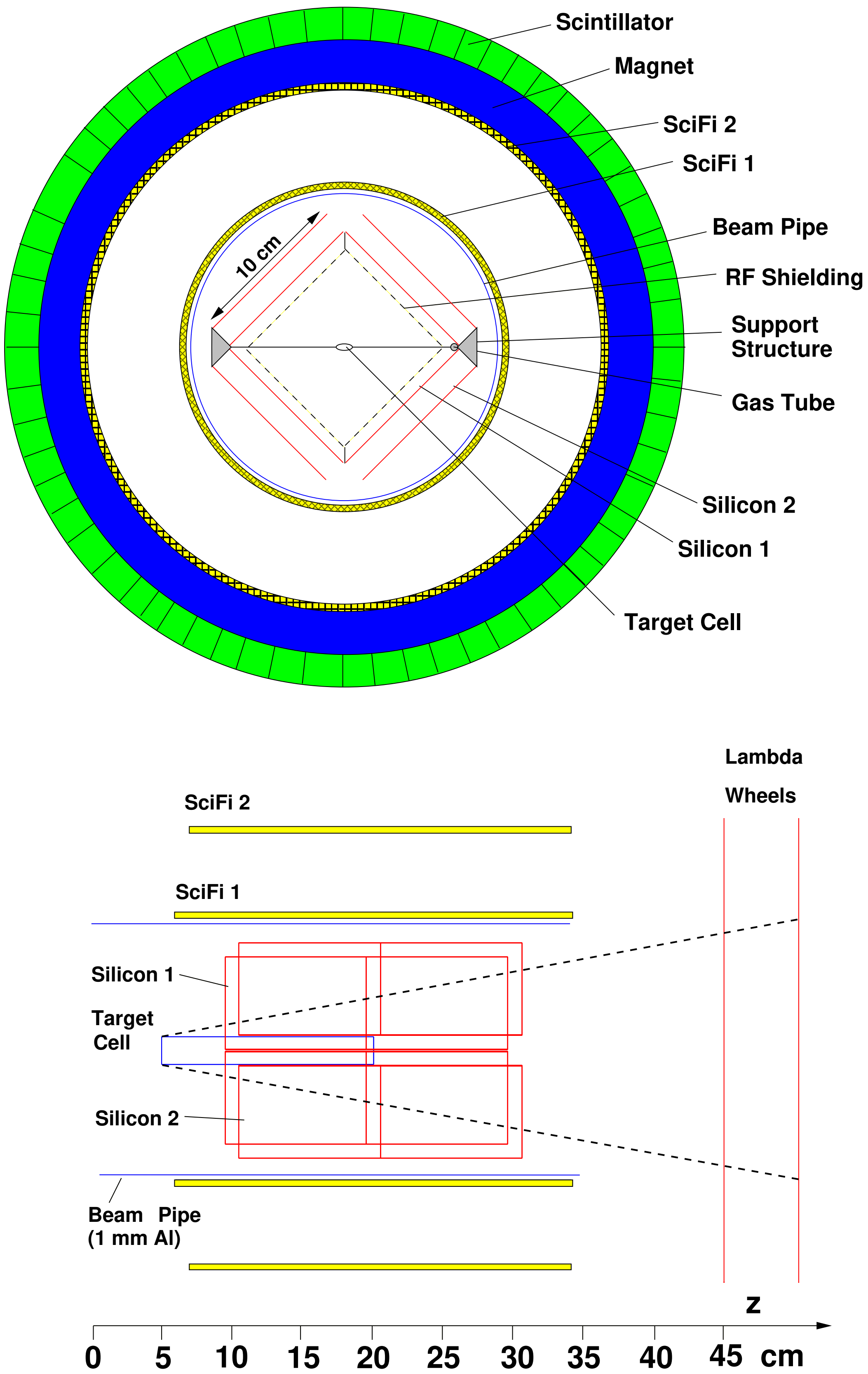

Fig. 16. Schematic cross section and topview of the HERMES Recoil Detector.

Figures 17 and 18 illustrate how well silicon and SciFi tracker complement one another. Together they cover practically the entire p-θ-plane, with a combined acceptance of 89% of all recoil protons (DVCS simulation). There is a relatively large overlap region, for recoil proton momenta between 260 and 500 MeV/c, where the information from both tracking detector can be combined.

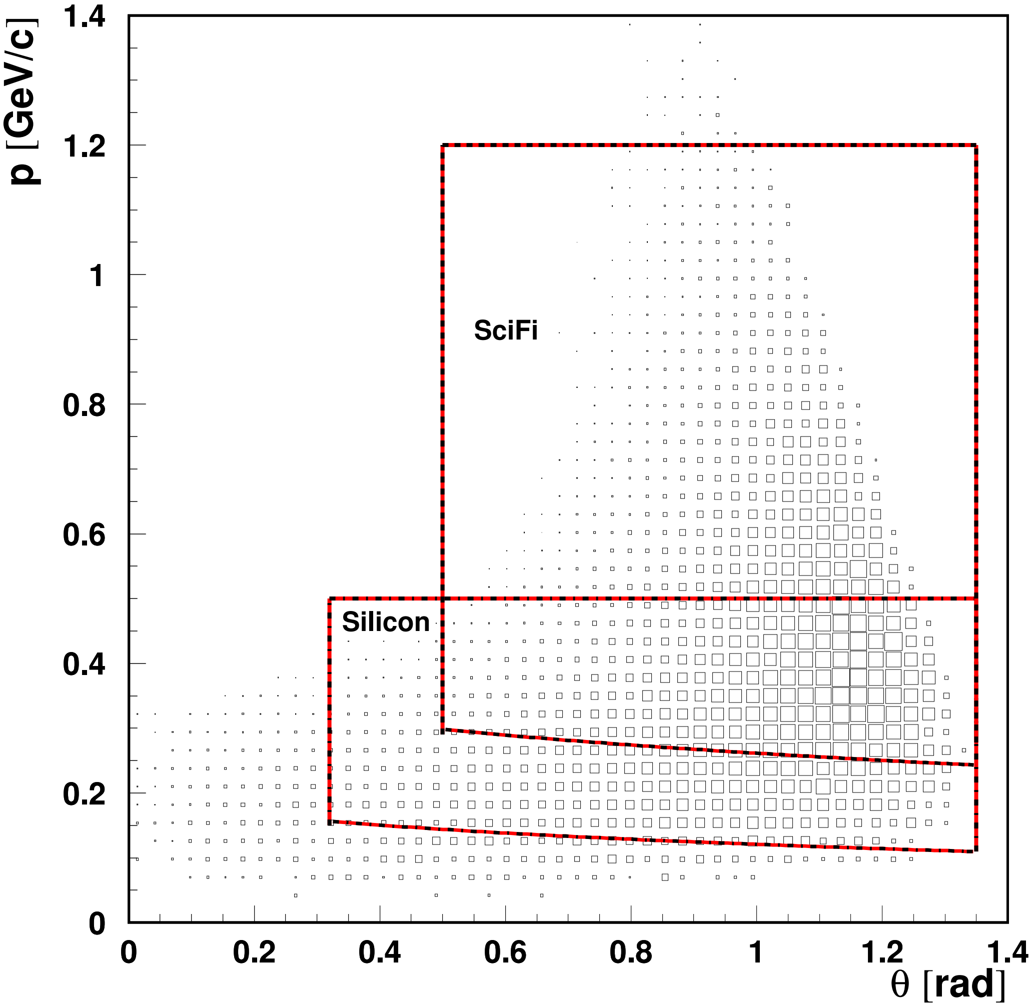

Fig. 17. Distribution of the recoil proton momentum p versus the polar angle θ for DVCS events. The two marked regions indicate the maximum acceptance of the Silicon tracker and the SciFi detector. Together they cover most of the data sample (89% of the statistics).

The pion/proton particle identification is provided by a combination of the momentum reconstruction from the SciFi tracker and the size of the signal in the silicon detector. As the silicon detector covers momenta up to 500 MeV/c most of the pions will be identified by not being detected in the silicon detector. For those particles that slip through the acceptance gaps of the silicon detector the sum of the signals in the SciFi tracker can be used for particle identification.

Figure 19 shows the acceptance of the Recoil Detector in $-t$. The left plot shows the $-t$ spectra accepted in the different detector components, while the right plot shows the normalised acceptance. It clearly illustrates that the silicon tracker adds the low $-t$-events below $-t = 0.06$ to the sample that will be particularly important for the extrapolation

$-t \to 0$. In addition, the silicon tracker will allow the measurement of ϕ_γ in this region, where it is difficult to extract from the real photon measurement.

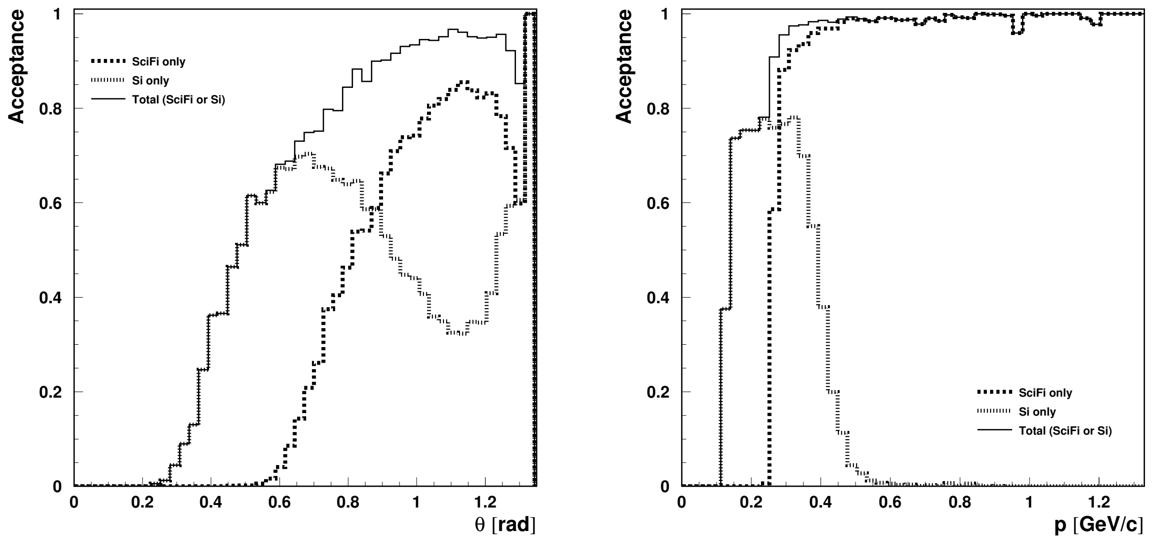

Fig. 18. Acceptance of the tracking detector in the polar angle θ (left) and in momentum p (right) for recoil protons from a simulated DVCS sample. The acceptance is shown separately for Silicon and SciFi detector and for both of them together. Two full space points are the minimum requirement.

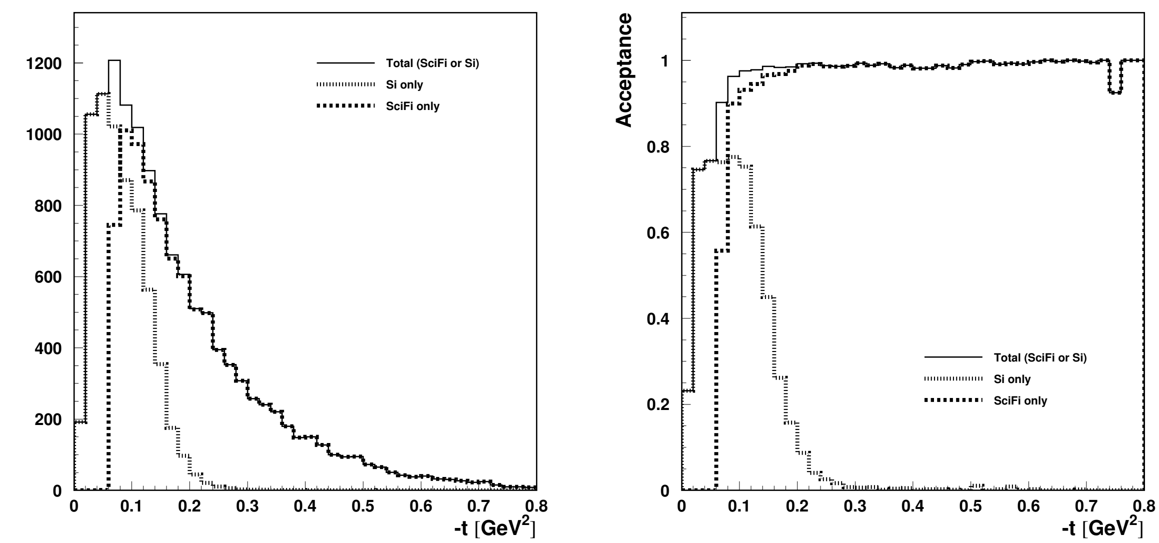

Fig. 19. Acceptance of the tracking detector in $-t$, the square of 4-momentum transfered to the recoil proton. Left: $-t$ spectra accepted in the different detector components. Right: Acceptance shown separately for Silicon and SciFi detector and for both of them together.

3.3 Expected Performance of the Recoil Detector

3.3.1 Monte Carlo Simulation

The most important measures of the expected performance of the Recoil Detector are its ability to reconstruct the momentum of the recoil proton, given by the relative momentum resolution $\Delta p/p$, and its absolute resolution in $-t$, Δt. Furthermore it is important to assess how well the exclusivity of a given data sample can be established.

In order to evaluate the performance of the Recoil Detector, a full Monte Carlo chain was required. Event samples have been generated for ρ-production, DVCS and ADVCS. Although all discussed processes have already been seen and analyzed at HERMES, this knowledge could only be used indirectly as the longitudinal proton momentum cannot be reconstructed from HERMES data. Exclusive ρ data have been simulated with the DIPSI event-generator. Although the Ryskin-model implemented in DIPSI [60,61] is a priori not valid at our kinematics, its parameters have been successfully adjusted to reproduce the semi-inclusive ω and ρ distributions in the HERMES acceptance. Hence this generator can also be used to simulate the performance of the Recoil Detector.

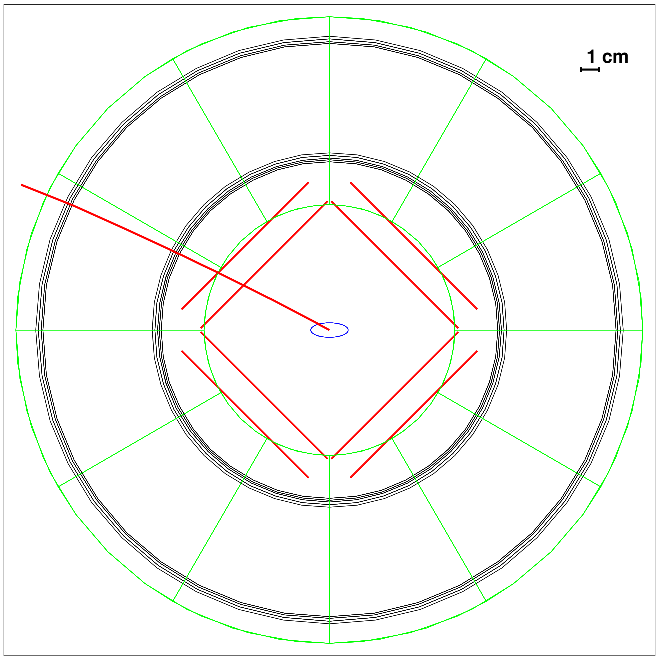

Fig. 20. Event display of the Recoil Detector MC simulation. The green (light gray) structure in the background represents the Λ-wheels. A recoil proton track is originating from the target.

For the DVCS and ADVCs samples a simple phenomenological model was used that simulates the cross section in x and Q^2 by assuming only a Q^2-dependence as

$$\frac{d\sigma}{dx\, dQ^2} \propto 1/Q^4 \tag{11}$$

The performance of the detector relies largely on the ability to detect missing transverse momentum. One main ingredient in this is the invariant mass of the hadronic state M_x (excluding the meson), which governs the momentum distribution of the undetected pion. M_x was chosen as the mass of the proton or the mass of the Δ, distributed according to its Breit-Wigner-shape, and t was generated with a slope of 6.5 GeV^{-2}, which is an average value for all exclusive processes seen at HERMES. The Δ-decay probabilities were assigned according to their isospin values and the decay distribution was assumed to be isotropic. It may not be isotropic in reality because it depends strongly on the density matrix element r^{04}_{33} [62], which is unknown at HERMES energies. However, it was checked that this has only a minor effect.

The output of either event generator was tracked through the forward spectrometer by the standard HERMES Monte Carlo (HMC). Exclusive events were selected and the corresponding recoil protons were processed separately by a GEANT3.21-based Recoil Detector Monte Carlo. An event display of the Recoil Detector MC is shown in figure 20.

3.3.2 Momentum Resolution

For the silicon detector and the SciFi tracker two different methods are used to measure the momentum of the recoil particles. The method for the silicon detector is based on the total energy deposition in both layers of silicon in combination with the reconstructed track direction. The method for the momentum reconstruction with the SciFi tracker on the other hand is based on the deflection of the particle tracks in the magnetic field. The resulting transverse momentum p_t of the particles in combination with the polar angle θ yields all three components of the particle momentum. The precision of the momentum measurement with the silicon detector is limited by the statistical fluctuations in the energy deposition. For the SciFi tracker this limit results mostly from the magnitude of the longitudinal magnetic field and from the multiple scattering in the material in front of the detector and in the inner SciFi detector (cf. figure 15).

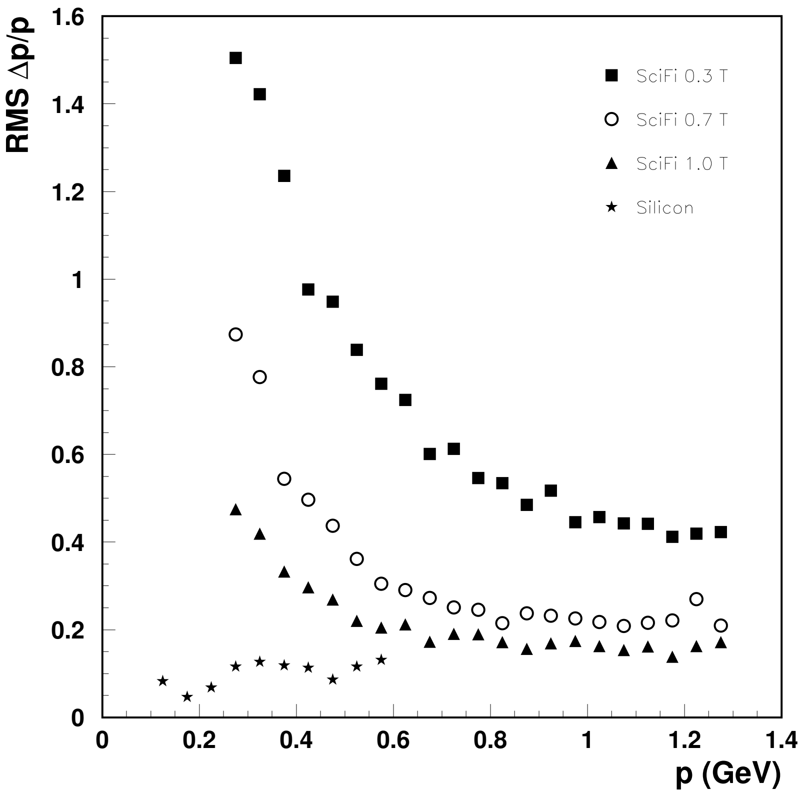

Fig. 21. Momentum resolution $\Delta p/p$ for recoil protons in the silicon tracker and the SciFi detector (for magnetic fields of 0.3, 0.7, and 1.0 T). Δp is here defined as the RMS of the distribution p(reconstructed) − p(true).

For the study of the performance of the detector data samples of DVCS, ADVCS and exclusive ρ-production were generated. The results for the momentum resolution for silicon tracker and SciFi detector (for three different magnetic fields) are shown in figure 21. The momentum resolution from the silicon tracker is of the order of 10-15%. For a B-field of 1.0 T the SciFi tracker has a resolution of about 20%, for 0.7 T only of 30%. Lower values lead to resolutions that are not acceptable. This suggests to use a B-field of 1.0 T if possible, leading to a relatively homogeneous resolution over the entire momentum range.

3.3.3 Resolution in t

The recoil particle 4-momentum $\mathrm{p_{rec}}$ can be used to determine the value of $-t$ via the relation

$$-t = (\mathrm{p_{rec}} - \mathrm{p_0})^2 \tag{12}$$

Since the initial proton is at rest ($\mathrm{p_0} = (\mathrm{m_p}, 0, 0, 0)$), the accuracy of the determination of $-t$ from the recoil proton depends only on the resolution of the particle momentum, not its direction. It follows that for events with low momentum recoil protons the good energy resolution of the silicon counter determines the resolution in $-t$. For low values of $-t$ this leads to an improvement of the resolution by about an order of magnitude compared to the result from the forward spectrometer. At medium values of $-t$ (0.15-0.5), where increasingly the SciFi detector will be used (cf. fig. 19), the $-t$-resolution using the recoil detector is improved by a factor of two for DVCS and comparable for ρ-production. This is illustrated in figure 22 for a sample of DVCS and exclusive ρ MC data.

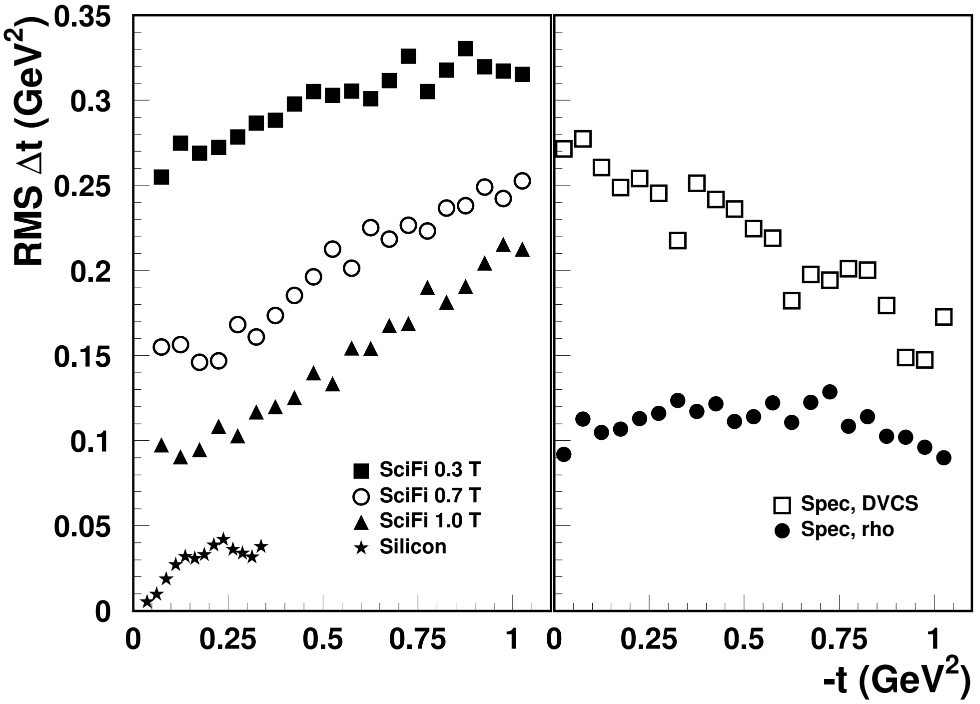

Fig. 22. Resolution in $-t$ (absolute values) for the silicon tracker, the SciFi detector (for different B-fields) and for the forward spectrometer (DVCS and ρ-data). The large improvement at low values of $-t$ due to the silicon tracker is clearly visible.

The improved resolution at low values of $-t$ coincides with the kinematic region where the t-dependence of the DVCS cross section is steepest, and a good resolution is most important. The Recoil Detector has the potential not only to significantly reduce the resonant background processes, but also to improve the accuracy of the measurement in the most important kinematic region. While at higher values of $-t$ (or recoil particle momentum) the improvement in resolution is less, the rejection of background events to the exclusive process is nonetheless essential to reduce the systematic error. Furthermore, the $-t$-dependence of the cross section is shallower at higher values of $-t$, so that an improved $-t$ resolution is less important than at low $-t$.

3.3.4 Background Suppression

Figure 23 illustrates how a coplanarity test can be used in a DVCS analysis to suppress the background from ADVCS events. The coplanarity test uses a combined cut in the two variables ω and R, where ω is defined as the angle between the missing transverse momentum and the measured transverse momentum of the recoil proton, while R is the ratio of their respective absolute values [63]. For the given MC data sample of DVCS and ADVCS events the silicon detector has been used for the momentum reconstruction where possible, otherwise the SciFi detector was used. The arrows indicate the preliminary cuts; the distributions in figure 23 have been normalised to unity.

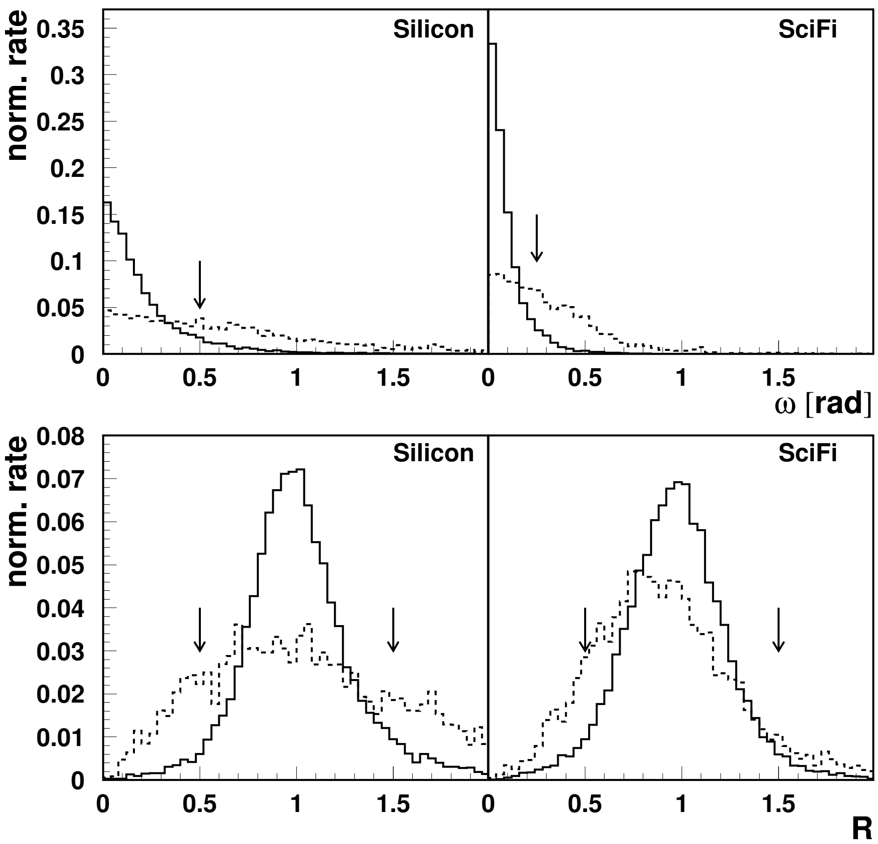

Fig. 23. Coplanarity cut using the two variables ω and R, where ω is defined as the angle between the missing transverse momentum and the measured transverse momentum of the recoil proton, while R is the ratio of their respective absolute values. The arrows indicate the cuts; the distributions for DVCS (solid) and ADVCS (dashed) have been normalised to unity.

As a result of this coplanarity cut about 84% of the DVCS events with detected recoil protons are kept in the sample, compared to a contamination from 33% of the corresponding ADVCS events. If this is combined with the detector acceptances that are different for nucleons from DVCS and ADVCS the overall efficiency of this cut for DVCS becomes 74%, with a contamination of only 14% of the ADVCS events. The coplanarity cut has not yet been optimised and an improvement in its performance can still be expected.

A second example for background suppression with the recoil detector is the case of exclusive π^+ production

$$ep \rightarrow e\pi^+ n \tag{13}$$

The main background consists of reactions with intermediate Δ^0 states

$$ep \rightarrow e\pi^+ \Delta^0 \tag{14}$$

with the consecutive decay of the Δ^0 in

$$\Delta^0 \rightarrow \pi^- p \qquad \text{or} \qquad \Delta^0 \rightarrow \pi^0 \text{n} \tag{15}$$

As the Recoil Detector will be effectively blind to neutrons, this background can already be suppressed if only one of the reaction products is detected. For a missing mass below 1.4 GeV, 61% of the negative pions and 62% of the protons from the Δ^0-decays are detected in the Recoil Detector. As the identification of either one of them is sufficient to reject the event, 87% of this background can be suppressed using the information of the Recoil Detector alone. The use of the Λ-wheels for the same purpose would lead to a suppression of only about 20% of this background. However, if the information of the Recoil Detector and the Λ-wheels is combined about 93% of all $\Delta^0 \rightarrow \pi^- p$ events can be rejected. The suppression of the $\pi^0 n$-background will depend on the efficiency of the π^0 detector, which has not yet been included in the Recoil Detector Monte Carlo.

4 Background Test Experiment

A scintillating fibre recoil test detector is currently being set up for insertion into the transverse magnet chamber for the running period of 2002. The goal of this test experiment is to study the background conditions in the target chamber, i.e. the contributions from Møller electrons, synchrotron radiation and from positrons from the beam halo scattering off the collimator upstream of the target cell. With a deuteron target it would also be possible to detect spectator protons, as was shown by the silicon test counter (cf. figure 1). Due to the small acceptance of the test detector the expected rate of recoil protons will be low, around two events per day. The test will also be used to understand the signals the various event types produce in the fibre detector and to optimise the suppression of background events.

The test detector consists of a 25 cm long scintillating fibre detector with 128 fibres of 0.5 mm diameter, arranged in a 16x8 pattern. Eight fibres are read out as one ‘road’, yielding 16 channels, which are fed to a Hamamatsu 16-channel PMT. In addition, three 3 mm thick trigger scintillators are placed underneath the fibre detector, with lengths of 5 cm, 8cm and 12 cm. Their signals are fed into PMTs.

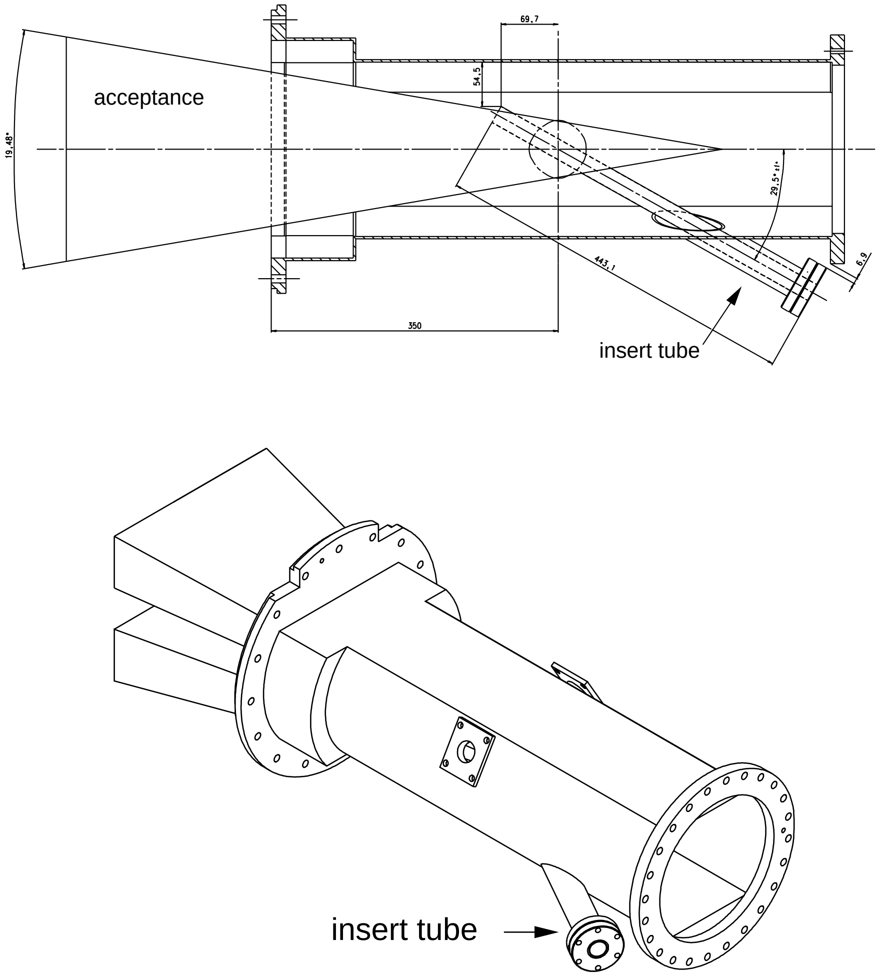

Fig. 24. Top view and 3d-view of the modified transverse target chamber with the insert for the scintillating fibre detector of the background test experiment.

The scintillating fibre detector is inserted into a tube in the transverse magnet chamber (cf. figure 24). The insert tube consists of a 40 cm long steel cylinder of 2.25 cm outer diameter with 0.15 mm wall thickness. It is inserted under an angle of 30 degrees from the upstream left side of the chamber, at a constant distance of 5.6 cm below the y=0 plane. It crosses the center of the target (x=z=0) and ends at z=7 cm. The insert tube stays completely outside of the standard HERMES acceptance.

The steel pipe of the insert has the thinnest off-the-shelf commercially available wall thickness. It is strong enough to hold the air pressure of one atmosphere inside against the vacuum of the target chamber outside, and to withstand moderate stress from inserting and extracting the test detector, which will be minimised by a rail- and guiding-system. On the other hand, protons will be stopped up to momenta of approximately 140 MeV/c, equivalent to a minimum $-t$ for recoil protons of 0.02 GeV^2. This cutoff is comparable to the one for protons that leave signals in both layers of the Silicon detector of the Recoil Detector.

5 Organisation

The different components of the Recoil Detector project have been distributed between the presently involved institutes. This envisaged distribution is of course subject to the availability of funds and manpower. Additional groups may still join the project which also could still lead to changes in the list of responsibilities. Each component has one responsible institute and can have additional contributing institutes. In the case of the Silicon Detector, the responsibility is shared between Zeuthen and Glasgow, with an internal distribution of the respective sub-tasks.

Component	Institutes
Target, Beam Pipe, Collimator, Infrastructure	**Erlangen**
Silicon Detector	**Zeuthen, Glasgow** Erlangen
SciFi Detector	**Giessen**
Magnet incl. Mapping	**Protvino**
π^0-Detector	**Gent**, Glasgow
Monte Carlo	**Erlangen**, Glasgow
Software, Reconstruction	**Glasgow**, Erlangen Giessen, Zeuthen
Background Test Experiment	**Erlangen**, Zeuthen
Silicon Test Experiment	**Erlangen**, Glasgow Zeuthen
SciFi Test Experiment	**St.Petersburg**, Giessen
Project Management	**Glasgow**

Table 2
Overview of the key components of the project and the distribution of responsibilities between the institutes. Boldface indicates the main responsible institute.

References

[1] HERMES Collaboration, "New silicon-detector systems for the HERMES front region", DESY-PRC 97-06, HERMES 97-032

[2] K. Fiedler, "Identification of Spectator Nucleons at HERMES", PhD thesis, University of Erlangen-Nürnberg, March 2001

[3] M. van Beuzekom et al., Nucl. Instr. Meth. **A409** (1998) 255

[4] F. Krautschneider, "Photoproduction of negative Pi-mesons between 900 MeV and 1800 MeV", PhD thesis, University of Bonn, 1976

[5] W-J. Kasdorp et al, Few-Body Syst. **25** (1998) 115

[6] K.I. Blomqvist et al, Phys. Lett. **B424** (1998) 33

[7] E.L. Berger and D. Jones, Phys. Rev. **D23** (1981) 1521

[8] J.P. Guillet, Z. Phys. **C39** (1988) 75

[9] HERMES Collaboration, "The HERMES Charm Upgrade Program: A Measurement of the Double Spin Asymmetry in Charm Leptoproduction", Proposal to DESY-PRC, HERMES 97-004, and references therein

[10] W. Melnitchouk and A. Thomas, Phys. Lett. **B337** (1996) 11

[11] W. Melnitchouk, A.W. Schreiber and A.W. Thomas, Phys. Rev. **D49** (1994) 1183

[12] W. Melnitchouk, M. Sargsian and M.I. Strikman, Z. Phys. **A359** (1997) 99

[13] M. Dittes et al., Phys. Lett. **B209** (1988) 325

[14] D. Mueller et al., Fortsch. Phys. **42** (1994) 101

[15] A.V. Radyushkin, Phys. Lett. **B385** (1996) 333

[16] X. Ji, Phys. Rev. Lett. **78**, 610 (1997), Phys. Rev. **D55** (1997) 7114

[17] HERMES Collaboration, A. Airapetian et al., Eur. Phys. Journ. **C17** (2000) 389

[18] HERMES Collaboration, A. Airapetian et al., hep-ex/0102037 and DESY-00-189

[19] HERMES Collaboration, A. Airapetian et al., hep-ex/0104005 and DESY-01047.

[20] HERMES Collaboration, A. Airapetian et al., "Measurement of the Beam-Spin Azimuthal Asymmetry Associated with Deeply-Virtual Compton Scattering", in preparation

[21] G. P. Lepage and S. J. Brodsky, Phys. Lett. **B87** (1979) 359

[22] A. V. Radyushkin, Phys. Lett. **B380** (1996) 417

[23] X.-D. Ji and J. Osborne, Phys. Rev. **D58** (1998) 094018

[24] J.C. Collins and A. Freund, Phys. Rev. **D59** (1999) 074009

[25] M. Diehl, T. Gousset, B. Pire and J. P. Ralston, Phys. Lett. **B411** (1997) 193

[26] M. Vanderhaeghen, P. A. M. Guichon, M. Guidal, Phys. Rev. **D60** (1999) 094017

[27] J. Ely, private communication

[28] A.V. Belitsky et al., Nucl. Phys. **B593** (2001) 289

[29] V. Korotkov, W.-D. Nowak, in preparation

[30] M. Kolstein, "Exclusive rho0 - Meson Electroproduction at HERMES", PhD Thesis, Vrije Universiteit Amsterdam, Netherlands, 1998

[31] M. Tytgat, "Diffractive Production of rho0 and omega Vector Mesons at HERMES", PhD thesis, Universiteit Gent, 2000

[32] G. Rakness, "Spin Polarization Transfer in Exclusive Phi Electroproduction", PhD thesis, University of Colorado at Boulder, 2000

[33] F. Meissner, "Measurement of the J/psi Cross Section and Double-Spin Asymmetries in Vector Meson Production in Polarised Lepton-Nucleon Scattering at HERMES", PhD thesis, Humboldt-Universität zu Berlin, 2000

[34] HERMES Collaboration, K. Ackerstaff et al., hep-ex/0002016

[35] L. Frankfurt, W. Koepf, M. Strikman, Phys. Rev. **D54** (1996) 3194

[36] M. R. Adams et al., E665 Collaboration, Z. Phys. **C74** (1997) 237

[37] H. Holtmann et al., Z. Phys. **C69** (1996) 297

[38] K. Negodaeva, priv. comm.

[39] J. Collins, L. Frankfurt and M. Strikman, Phys. Rev. **D56** (1997) 2982

[40] L. Mankiewicz, G. Piller and T. Weigl, Eur. Phys. J. **C5** (1998) 119, Phys. Rev. **D59** (1999) 017501

[41] J. Volmer et al., Phys. Rev. Lett. **86** (2001) 1713 and references therein

[42] L.L. Frankfurt, M.V. Polyakov, M. Strikman and M. Vanderhaegen, Phys. Rev. Lett. **84** (2000) 2589

[43] M.I.Eides, L.L.Frankfurt and M.Strikman, Phys. Rev. **D59** (1999) 114025

[44] B. Lehmann-Dronke, A. Schaefer, M.V. Polyakov, K. Goeke, Phys.Lett. **B475** (2000) 147; hep-ph/0012108

[45] R.L. Jaffe, Phys. Rev. **D54** (1996) 6581

[46] M. Burkardt and R.L. Jaffe, Phys. Rev. Lett. **70** (1993) 2537

[47] J.Ellis, D.Kharzeev, A.Kotzinian, Z. Phys. **C69** (1996) 467

[48] S. Belostotski, Nucl. Phys. **B79** (Proc. Suppl.) (1999) 526

[49] S. Belostotski, Czech. J. Phys. **50** (2000) 45

[50] P. Astier et al., NOMAD Collaboration, Nucl. Phys. **B588** (2000) 3

[51] S.Willocq et al., WA59 Collaboration, Z. Phys. **C53** (1992) 207

[52] M. Guidal et al., Jefferson Lab proposal E99-105

[53] F. Sabatie et al., Jefferson Lab proposal E00-110

[54] N. d'Hose et al., 'Letter of Intent: DVCS at COMPASS', DAPNIA-CSTS-99, December 1999

[55] M. Rueter, DESY-ZM1, priv. comm.

[56] M. Hilgers, R. Horisberger, hep-ex/0101023

[57] W.Lange, priv. comm.

[58] H. Leich, R. Nahnhauer, R. Shanidze, DESY 98-002, physics/9801004

[59] E.C. Aschenauer et al., Nucl. Instr. Methods, A434(1999) 459

[60] M. Arneodo, L. Lamberti and M. Ryskin, Comput. Phys. Commun. **100** (1997) 195

[61] M. G. Ryskin, Z. Phys. **C57** (1993) 89

[62] K. Wacker et al., Nucl. Phys. **B144** (1978) 269

[63] B. Krauss, Diplom Thesis, University of Erlangen-Nürnberg, Oct.2000